Two novel heteropolymer-forming proteins maintain multicellular shape of the cyanobacterium *Anabaena* sp. PCC 7120

Benjamin L. Springstein[1*#], Dennis J. Nürnberg[2,†], Christian Woehle[1¥], Julia Weissenbach[1,‡], Marius L. Theune[1], Andreas O. Helbig[3], Iris Maldener[4], Tal Dagan[1], Karina Stucken[5*]

[1] Institute of Microbiology, Christian-Albrechts-Universität zu Kiel, Kiel, Germany

[2] Department of Life Sciences, Imperial College, London, United Kingdom

[3] AG Proteomics & Bioanalytics, Institute for Experimental Medicine, Christian-Albrechts-Universität zu Kiel, Kiel, Germany

[4] Interfaculty Institute of Microbiology and Infection Medicine Tübingen/Organismic Interactions, University of Tübingen, Tübingen, Germany

[5] Department of Food Engineering, University of La Serena, La Serena, Chile.

[#] Present address: Department of Microbiology, Blavatnick Institute, Harvard Medical School, Boston, MA, USA

[†] Present address: Institute of Experimental Physics, Free University of Berlin, Berlin, Germany

[¥] Present address: Max Planck-Genome-centre cologne, Max Planck Institute for Plant Breeding Research, Cologne, Germany

[‡] Present address: Faculty of Biology, Technion-Israel Institute of Technology, Haifa, Israel

* Corresponding authors: BLS: benjamin_springstein@hms.harvard.edu

KS: kstucken@userena.cl

Abstract

Polymerizing and filament-forming proteins are instrumental for numerous cellular processes such as cell division and growth. Their function in stabilization and localization of protein complexes and replicons is achieved by a filamentous structure. Known filamentous proteins assemble into homopolymers consisting of single subunits – e.g. MreB and FtsZ in bacteria – or heteropolymers that are composed of two subunits, e.g. keratin and α/β tubulin in eukaryotes. Here, we describe two novel coiled-coil-rich proteins (CCRPs) in the filament forming cyanobacterium *Anabaena* sp. PCC 7120 (hereafter *Anabaena*) that assemble into a heteropolymer and function in the maintenance of the *Anabaena* multicellular shape (termed trichome). The two CCRPs – Alr4504 and Alr4505 (named ZicK and ZacK) – are strictly interdependent for the assembly of protein filaments *in vivo* and polymerize nucleotide-independently *in vitro*, similar to known intermediate filament (IF) proteins. A Δ*zicK*Δ*zacK* double mutant is characterized by a zigzagged cell arrangement and hence a loss of the typical linear *Anabaena* trichome shape. ZicK and ZacK interact with themselves, with each other, with the elongasome protein MreB, the septal junction protein SepJ and the divisome associate septal protein SepI. Our results suggest that ZicK and ZacK function in cooperation with SepJ and MreB to stabilize the *Anabaena* trichome and are likely essential for the manifestation of the multicellular shape in *Anabaena*. Our study reveals the presence of filament-forming IF-like proteins whose function is achieved through the formation of heteropolymers in cyanobacteria.

Introduction

Cytoskeletal proteins that polymerize to form protein filaments are paramount in bacterial cell biology where they play a role in cell division, alignment of bacterial microcompartments (BMCs), chromosome and plasmid segregation, organization of cell polarity and the determination of cell shape (Wagstaff and Löwe, 2018). For example, FtsZ (Van De Putte *et al.*, 1964; de Boer *et al.*, 1992), the prokaryotic homolog to the eukaryotic tubulin (Löwe and Amos, 1998; Nogales *et al.*, 1998), is a main component of the divisome (den Blaauwen *et al.*,

2017), a multiprotein complex that governs cell division in bacteria and self-assembles into a proteinaceous ring (called Z-ring) at the midcell position (Bi and Lutkenhaus, 1991). Another key bacterial cytoskeletal protein is MreB (Jones *et al.*, 2001), which is a homolog of the eukaryotic actin (de Boer *et al.*, 1992; Ent *et al.*, 2001) and a crucial component of the multi-protein complexes termed the elongasome. This complex modulates cell elongation in many rod-shaped bacteria through regulating peptidoglycan (PG) biogenesis (Errington and Wu, 2017). Both, FtsZ and MreB monomers assemble into filamentous strands (protofilaments), consisting of only one type of monomer, termed homopolymers (Wagstaff and Löwe, 2018). The cell division in prokaryotes markedly contrasts the division of plastid organelles in photosynthetic eukaryotes that are of cyanobacterial origin (e.g., (Dagan *et al.*, 2013)). Cell division in plastids is dependent on the cooperative function and heteropolymerization of two FtsZ homologs, FtsZ1 and FtsZ2 in the green lineages and FtsZA and FtsZB in the red lineage. However, each FtsZ homolog is also self-sufficient to form homopolymers (reviewed by (Chen *et al.*, 2018)). In contrast, a likely horizontally transferred pair of tubulin homologs, BtubA and BtubB from *Prothescobacter* spp., exclusively assembles into heteropolymers *in vitro* (Schlieper *et al.*, 2005), revealing similar properties than eukaryotic microtubules that are heteropolymers composed of α and β tubulin monomers (Alberts *et al.*, 2014). Eukaryotic IF proteins, despite sharing substantially the same building blocks and a high degree of coiled-coil (CC) domains (Fuchs and Weber, 1994), which are considered excellent mediators of protein-protein interactions (Mason and Arndt, 2004), only form heteropolymers with a subset of other IF proteins within their same assembly group but otherwise form obligate homopolymers (Herrmann and Aebi, 2000).

Polymer-forming coiled-coil-rich proteins (CCRPs) have been shown to play a role also in multicellularity traits in myxobacteria and actinomycetes (reviewed by (Lin and Thanbichler, 2013; Wagstaff and Löwe, 2018)). Similar to eukaryotic IFs (Fuchs and Weber, 1994), many bacterial CCRPs perform cytoskeletal functions through their ability to self-assemble into filaments *in vivo* and *in vitro* in a self-sufficient and co-factor independent manner (Ausmees *et al.*, 2003; Bagchi *et al.*, 2008; Specht *et al.*, 2011; Holmes *et al.*, 2013). The CCRP

Crescentin determines the *C. crescentus* typical curved morphology by aligning to the inner cell curvature and exuding local mechanical constrains on the PG biosynthesis, likely through cooperation with MreB (Ausmees *et al.*, 2003; Charbon *et al.*, 2009). In analogy to eukaryotic IF proteins, Crescentin assembles into straight protein filaments with a width of 10 nm and displays a similar domain organization (Ausmees *et al.*, 2003). However, while Crescentin is often considered a prokaryotic homologue to eukaryotic IF proteins, its restricted distribution to only one identified organism questions real homologous relationships and rather suggests that it was acquired by horizontal gene transfer (Erickson, 2007; Wickstead and Gull, 2011). Multicellular actinobacteria, such as *Streptomyces* spp., grow by building new cell wall (*i.e.*, PG) only at the cell poles, independent of MreB (Letek *et al.*, 2008), a striking different cell growth than in most other bacteria (Surovtsev and Jacobs-Wagner, 2018). This characteristic polar growth mode is organized by a cytoskeletal network of at least three CCRPs - DivIVA, Scy and FilP – that directly interact with each other to form the polarisome (Holmes *et al.*, 2013). FilP and Scy, independently self-assemble into filaments *in vitro* (Bagchi *et al.*, 2008; Holmes *et al.*, 2013; Javadi *et al.*, 2019), thereby fulfilling major IF-like criteria (Wagstaff and Löwe, 2018). *In vivo*, however, Scy does not form filaments and instead accumulates as foci at future branching points (Holmes *et al.*, 2013), while FilP localizes as gradient-like caudates at the hyphal tips (Fröjd and Flärdh, 2019), instead of forming distinct filaments as observed for Crescentin (Ausmees *et al.*, 2003). Although of essential importance for growth and cell shape, the polarisome does not directly regulate multicellularity in Actinobacteria, which is instead maintained by the highly reproducible and coordinated formation of Z-ring ladders during sporulation (Schwedock *et al.*, 1997; Claessen *et al.*, 2014).

Among prokaryotes, Cyanobacteria exhibit the largest morphological diversity, comprising unicellular species as well as complex cell-differentiating multicellular species (Rippka *et al.*, 1979). For the model multicellular cyanobacterium *Anabaena*, it is imperative to form stable trichomes in order to cope with external influences such as shearing stress (Corrales-Guerrero *et al.*, 2013; Flores *et al.*, 2016). Under nitrogen-deprived growth conditions, *Anabaena* develops specialized cell types for nitrogen fixation (heterocysts), which

are evenly spaced among the *Anabaena* trichome and provide other vegetative cells with fixed nitrogen compounds like glutamine (Herrero *et al.*, 2016). In *Anabaena*, proteinaceous cell-joining structures that allow intercellular transport (*i.e.*, cell-cell communication) and function by gating are termed septal junctions (analogous to eukaryotic gap junctions; (Wilk *et al.*, 2011; Flores *et al.*, 2018; Weiss *et al.*, 2019)). Septal junctions consist of several structural elements, an intracellular cap, a plug inside the cytoplasmic membrane formed by the septal junction protein FraD and a tube traversing the septum through nanopores in the peptidoglycan (Weiss et al. 2019). The correct positioning of the septal protein SepJ, which is involved in septum maturation and filament stability, among others, dependents on the FtsZ-driven divisome component FtsQ (Ramos-León *et al.*, 2015), which links the early and late assembly components of the divisome (Choi *et al.*, 2018). FtsZ was shown to be essential for *Anabaena* viability and to assemble in a typical Z-ring structure at future septum sites in vegetative cells while being downregulated in heterocysts (Zhang *et al.*, 1995; Sakr *et al.*, 2006a; Klint *et al.*, 2007). In contrast, MreB is dispensable for *Anabaena* viability but determines the typical rectangular-like, since Δ*mreB* mutant cells show pronounced rounded and swollen morphotype. Unlike in many unicellular bacteria, MreB does not affect chromosome segregation, which was found to be governed, at least in part, by random segregation in *Anabaena* (Hu *et al.*, 2007). Maintenance of the rectangular cell shape is furthermore dependent on a class B penicillin-binding-protein (PBP) (Burnat *et al.*, 2014) and AmiC-type cell wall amidases in *Anabaena* (Bornikoel *et al.*, 2017; Kieninger *et al.*, 2019), suggesting that loss of normal cell shape is commonly associated with defects in PG biogenesis (Fenton *et al.*, 2016).

In this work, we aimed to identify proteins that play a role in cyanobacterial morphology and multicellularity. Searching for IF-like CCRPs, we identified two novel CCRPs in *Anabaena* that are capable of assembly exclusively into a heteropolymer *in vitro* and *in vivo* and that have a putative role in the *Anabaena* linear trichome shape.

Results

CCRPs ZicK and ZacK from *Anabaena* are conserved in Cyanobacteria

A computational survey of the *Anabaena* genome for protein-coding genes containing a high coiled-coil content (Springstein *et al.*, 2020b) revealed two CCRPs Alr4504 and Alr4505; here we term the two CCRPs ZicK and ZacK, respectively (that is, zig and zag in German). ZicK is predicted to contain five distinct coiled-coil (CC) domains while ZacK has four CC domains (Fig 1A; Supplementary File 1). Using PSORTb (v.3.0.2), both ZicK and ZacK are predicted to be cytoplasmic proteins, which is corroborated by the absence of detectable transmembrane domains (predicted using TMHMM v. 2.0). Since both proteins (and their homologs) are annotated as hypothetical proteins (Supplementary File 2), we validated their transcription under standard (BG11) and diazotrophic ($BG11_0$) growth conditions (Supplementary Fig. 1B,C). The genomic neighbourhood of *zicK* and *zacK* motivated us to test for a common transcriptional regulation of both genes (*i.e.*, an operon structure), however, we did not identify a common transcript (using RT-PCR; Supplementary Fig. 1A,B). Searching for known proteins sharing structural similarities to ZicK/ZacK using I-TASSER revealed structural similarities between ZicK and the eukaryotic cytolinker protein plectin, and of ZacK with the cell division protein EzrA, a predicted structural similarity that was previously associated with other bacterial CCRPs, including Crescentin, $HmpF_{Syn}$ and $HmpF_{Syc}$ (Springstein *et al.*, 2020b). Further annotation using the NCBI conserved domain search (Marchler-Bauer *et al.*, 2016) showed that ZicK and ZacK contain “structural maintenance of chromosomes” (SMC) domains (Fig. 1B), similarly to what we previously identified in other self-polymerizing cyanobacterial CCRPs (Springstein *et al.*, 2020b). A search for ZicK/ZacK homologs by sequence similarity revealed that they are absent in picocyanobacteria (*i.e.*, *Synechococcus*/*Prochlorococcus*) and generally rare in unicellular cyanobacteria. Otherwise, about 50% of the examined 168 cyanobacterial genomes have homologs for the two genes (Fig. 1C and Supplementary File 2). Several heterocystous cyanobacteria lacking ZacK/ZacK homologs are characterized by a reduced genome (e.g., *Nostoc azollae* PCC 0708 and *Richelia intracellularis*). Additionally,

Chlorogloeopsis spp. that forms multiseriate filaments is lacking the homologs and several strains of *Fischerella* spp., which forms true branching filaments, harbour only a ZacK homolog. The protein sequence of ZicK and ZacK homologs is well conserved, with about 55% amino acids identity among the homologs. The number of CC domains, however, differ among ZicK and ZacK homologs: between 3-6 CC domains in ZicK homologs, and 3-10 domains in ZacK homologs (Supplementary File 1). Notably, ZicK and ZacK are neighbours in 53 out 72 genomes; both proteins and their genomic neighbourhood is highly conserved among heterocystous cyanobacteria (Fig. 1C,D).

ZicK and ZacK are interdependent for polymerization *in vitro*

As a prerequisite for proteins to be considered as IF-like proteins, it is imperative for them to be able to self-interact *in vivo* and to polymerize into long protein filaments *in vitro* (Wagstaff and Löwe, 2018). To investigate the *in vitro* polymerization properties of ZicK and ZacK, we employed an *in vitro* polymerization assay that we previously established to test CCRPs' polymerization properties (Springstein *et al.*, 2020b). As a positive control for our approach, we used Crescentin (Fig. 1A), which formed an extensive filamentous network in our *in vitro* assay (Supplementary Fig. 2). As negative controls, we included empty vector-carrying *E. coli* cells, GroEL1.2 from *Chlorogloeopsis fritschii* PCC 6912 (known to form oligomers (Weissenbach *et al.*, 2017)) and the highly soluble maltose binding protein (MBP), all of which were tested negative for filament formation *in vitro* using our approach (Supplementary Fig. 2). Purified ZicK protein formed into amorphous, non-filamentous protein aggregates while ZacK assembled into aggregated sheet-like structures (Fig. 2A). The vast majority of ZacK protein precipitated into clumps of aggregates upon renaturation, which resembled the structures observed for GroEL1.2, suggesting that ZacK has only a partial capacity to self-polymerize or, more likely, is highly unstable on its own *in vitro*. Inspired by the close genomic localization of *zicK* and *zacK,* we next tested for a potential heteropolymerization of both proteins. This revealed that ZicK and ZacK co-assembled into a meshwork of protein heteropolymers upon co-renaturation (Fig. 2A, Supplementary Fig. 3). While both, ZicK and ZacK renatured alone,

187 formed aggregates in the dialysis tubes that were detectable with the naked eye (similar to our
188 observations from GroEL1.2), co-renatured ZicK/ZacK remained in solution, a common
189 property of eukaryotic IFs (Köster *et al.*, 2015). Next, we tested whether the co-filamentation
190 was dosage dependent and observed that distinct protein filaments could be detected *in vitro*
191 only with equal amounts of ZicK and ZacK (Supplementary Fig. 3). To further test for an *in vivo*
192 self-interaction, we analysed the self-binding capacity ZicK and ZacK using the bacterial
193 adenylate cyclase two-hybrid (BACTH) assay and found that ZicK and ZacK interact with
194 themselves and also with each other (Fig. 2B) confirming the heterologous binding capacity of
195 both proteins. Consequently, ZicK and ZacK fulfil a major characteristic of IF and IF-like
196 proteins as they are able to self-assemble into filament-like structures *in vitro*, although, unlike
197 other bacterial IF-like CCRPs, this assembly exclusively occurs as a heteropolymer.

198 **ZicK and ZacK are interdependent for polymerization *in vivo***

199 To examine the *in vivo* localization pattern of ZicK and ZacK, we initially expressed
200 translational GFP fusions of both proteins from the replicative pRL25C plasmid, which is
201 commonly used in experimental work in *Anabaena* (Sakr *et al.*, 2006b; Sakr *et al.*, 2006a; Hu
202 *et al.*, 2007; Du *et al.*, 2012). The expression of ZicK-GFP and ZacK-GFP from their respective
203 native promoters (as predicted using BPROM (Solovyev and Salamov, 2011)) revealed no
204 discernible expression of ZacK-GFP, while ZicK-GFP accumulated within the cells as dot-like
205 aggregates (Supplementary Fig. 4A). We assume that the lack of ZacK-GFP expression from
206 its predicted native promoter is based on the uncertainty of the precise promoter site prediction.
207 Alternatively, and although not expressed as an operon, expression of *zacK* could be affected
208 by the expression of *zicK* by so far unknown mechanisms. Consequently, we proceeded to
209 investigate the *in vivo* localization of both proteins from the copper-regulated *petE* promoter
210 (P_{petE}), which is commonly used to study the subcellular protein localization in *Anabaena* (e.g.,
211 FtsZ, MreB and SepI; (Sakr *et al.*, 2006a; Sakr *et al.*, 2006b; Hu *et al.*, 2007; Springstein *et al.*,
212 2020a). The expression of ZicK-GFP and ZacK-GFP from P_{petE} in *Anabaena* independently did
213 not reveal distinct or filamentous structures but resulted in the formation of inclusion body-like

aggregates within the cells (Fig. 3A), similar to those observed for P_{zicK}::*zicK-gfp* (Supplementary Fig. 4A). We could not detect any structures when we expressed ZicK and ZacK N-terminally fused to GFP, suggesting that the N-terminus is key for proper protein folding. Consequently, we next proceeded to co-express the two proteins with different fluorophores (from P_{petE}): ZicK C-terminally fused to eCFP (ZicK-eCFP) and ZacK C-terminally fused to GFP (ZacK-GFP). This revealed the formation of a ZicK/ZacK heteropolymer filament-like structure that usually localized along the longitudinal cell axis and in rare occasions also perpendicular to the cell axis (Fig. 3B). The prominent formation of the ZicK/ZacK heteropolymer was furthermore evident as electron-dense filament-like structures in ultrathin sections using electron microscopy (Fig. 3C). To confirm that the localization of fluorophore tagged ZicK and ZacK is not affected by the wild type (WT) *zicK* or *zacK* alleles, we additionally localized both proteins individually or together in a Δ*zicK*Δ*zacK* double mutant. These experiments revealed the same localization pattern as in *Anabaena* WT, suggesting that natively present ZicK or ZacK proteins do not affect the formation of ZicK-GFP, ZacK-GFP or the ZicK-eCFP/ZacK-GFP heteropolymer (Supplementary Fig. 4B,C). The intracellular localization of the ZicK/ZacK heteropolymer in *Anabaena* indicates that the polymer is either anchored at the cell poles or specifically split during cell division, as ZicK/ZacK filament-like structures were never observed to cross cell-cell borders and only traversed through not yet fully divided cells (Fig. 3B inlay and Fig. 3C). To further explore whether the ZicK/ZacK heteropolymer assembly is restricted to *Anabaena*, we proceeded to analyse ZicK and ZacK *in vivo* in an unrelated heterologous system using the *E. coli* split GFP assay (Wilson *et al.*, 2004). Clearly discernible filamentous-like structures (reminiscent of FilP-GFP (Bagchi *et al.*, 2008)) could be detected upon co-expression of ZicK and ZacK C-terminally fused to the split GFP products (ZicK-NGFP and ZacK-CGFP; Supplementary Fig. 5). This is in agreement with the lack of discernible structures upon expression of N-terminally GFP-fused ZicK and ZacK in *Anabaena* and is also in concert with the essential N-terminal domain for polymerization of IF and IF-like proteins (Heins and Aebi, 1994; Cabeen *et al.*, 2009; Cabeen *et al.*, 2011). Nonetheless, some indications for heteropolymerization were also present upon co-expression

of NGFP-ZicK with ZacK-CGFP, which is in agreement with the BACTH results that indicated that both, N and C-terminal fusions of ZicK and ZacK are potentially able to interact with each other (Fig. 2B). The different heteropolymerization phenotype of ZicK/ZacK polymer in *E. coli* and *Anabaena* suggests that there are other so far unknown factors that modulate the specific ZicK/ZacK heteropolymerization phenotype, as shown in the following section.

Deletion of *zicK* and *zacK* leads to defects in trichome and cell shape and *Anabaena* viability

In contrast to the obtained Δ*zicK*Δ*zacK* double mutant, single Δ*zicK* or Δ*zacK* mutant strains could not be generated, suggesting that the presence (or absence) of ZicK or ZacK alone is lethal for *Anabaena*. Further investigating the Δ*zicK*Δ*zacK* mutant phenotype revealed an altered trichome and cell shape phenotype and a reduced trichome viability (Fig. 4). Unlike the linear trichome growth pattern of the WT, the Δ*zicK*Δ*zacK* mutant strain grew as zigzagged trichomes (Fig. 4A), a phenotype that could be rescued by heterologous expression of P_{zicK}::*zicK-zacK* from pRL25C but not from P_{zicK}::*zicK-ecfp+zacK-gfp* (Supplementary Figs, 4C and 6A). Additionally, Δ*zicK*Δ*zacK* cells were significantly larger (WT: 27.42 ± 14.75 μm^3; Δ*zicK*Δ*zacK*: 32.52 ± 12.54 μm^3; P: <0.0001; Student's t test) and significantly more round (WT: 0.8063 ± 0.1317; Δ*zicK*Δ*zacK*: 0.8530 ± 0.1130; P: <0.0001; Student's t test) in comparison to the WT (Fig. 4B,C), reminiscent of the Δ*mreB* mutant strain (Hu *et al.*, 2007). The round and swollen cell phenotypes of the Δ*zicK*Δ*zacK* mutant strains are indicative of an impairment in cell wall integrity and/or defects in PG biogenesis as well as an elevated sensitivity to turgor pressure (Fenton *et al.*, 2016; Rojas and Huang, 2018). Consequently, we tested for an elevated sensitivity of the Δ*zicK*Δ*zacK* mutant to cell wall damaging enzymes. This showed that the Δ*zicK*Δ*zacK* mutant is slightly more sensitive to Proteinase K treatment but was unaffected by lysozyme treatment and still retained the ability to grow diazotrophically (*i.e.*, on $BG11_0$ plates) (Fig. 4D) and to form heterocysts (Supplementary Fig. 6B). More importantly, however, we found that the Δ*zicK*Δ*zacK* mutant lost the ability to grow in liquid culture (with and without agitation; Fig. 4E), which could be complemented with pRL25C

carrying P_{zick}::*zicK-zacK* (Supplementary Fig. 6C), hinting for an elevated sensitivity to fluid shear stress or turgor pressure.

ZicK and ZacK interact with proteins involved in cell shape and trichome integrity

Considering the impact of the deletion of *zicK* and *zacK* on cell and trichome shape and the assumed septal docking of the ZicK/ZacK heteropolymer, we next wanted to investigate whether both, ZicK and ZacK physically interact with other proteins known to function in cell shape determination and cell-cell communication. Using the BACTH assay, we found that both, ZicK and ZacK, interacted with the divisome-associated septal protein SepI (Springstein *et al.*, 2020a), the septal protein SepJ (Flores *et al.*, 2007), the cell shape-determining protein MreB as well an elongasome associated protein (ZipM; covered in more detail in subsequent study) and the *Anabaena* homolog to HmpF (here named $HmpF_{Ana}$), whose homologs were shown to be involved in motility in *Nostoc punctiforme* ATCC 29133 (Cho *et al.*, 2017) and *Synechocystis* sp. PCC 6803 (Bhaya *et al.*, 2001; Springstein *et al.*, 2020b) (Fig. 5A). No interactions were found with FtsZ, FraC and FraD (Supplementary Fig. 7). We attempted to further confirm our interaction results with affinity co-elution experiments but found that Ni-NTA-bound ZicK and ZacK purified from *E. coli* readily precipitated upon transfer from denaturing to native buffer conditions, precluding further co-elution studies. Additionally, we observed that non-denaturing conditions failed to purify overexpressed CCRPs from *E. coli*, confirming their inherent insoluble nature, a property known to eukaryotic IFs (Kelemen, 2017). Instead, we surveyed for further interaction partners by anti-GFP co-immunoprecipitation experiments of *Anabaena* cells expressing ZicK-GFP and analysed co-precipitated proteins by LC-MS/MS analytics (all 27 identified possible interactors are listed in Supplementary File 3). This analysis confirmed that ZicK and ZacK interact with each other *in vivo* and further strengthened the observed association of ZicK with MreB (Fig. 5B). Furthermore, ZicK co-precipitated ParA (Fig. 5B), a walker A-type ATPase, involved in chromosome and plasmid partitioning (Lutkenhaus, 2012) and All4051 (also termed AnAKb), a protein associated with low-temperature resistance and potentially involved in cryoprotectant production (Ehira *et al.*, 2005).

296 **Deletion of *zicK* and *zacK* affects the localization of MreB and the chromosomes**

297 As our BACTH analysis identified SepI and SepJ as interaction partners, and both proteins are
298 involved in intercellular transport and cell-cell communication in *Anabaena* (Mullineaux *et al.*,
299 2008; Springstein *et al.*, 2020a), we proceeded to test whether the Δ*zicK*Δ*zacK* mutant is also
300 affected in solute diffusion using fluorescence recovery after photobleaching (FRAP)
301 experiments of calcein stained Δ*zicK*Δ*zacK* mutant. However, this analysis did not reveal any
302 defect in cell-cell communication in the Δ*zicK*Δ*zacK* mutant (Supplementary Fig. 8A-C) and
303 hence ZicK and ZacK do not affect septal junction functionality. Additionally, electron
304 microscopy of ultrathin sections of the Δ*zicK*Δ*zacK* mutant, did not show any discernible
305 differences in the ultrastructure of the cells compared to cells of *Anabaena* WT (Supplementary
306 Fig. 8D). In accordance with a lack of interaction between FtsZ and ZicK/ZacK, FtsZ placement
307 was unaffected in the Δ*zicK*Δ*zacK* mutant as shown using anti-FtsZ immunofluorescence
308 (Supplementary Fig, 9A). Following the lead of ZicK/ZacK interaction partners, we next
309 analysed the localization of MreB in the *Anabaena* WT and the Δ*zicK*Δ*zacK* mutant using a
310 functional P_{petE}::*gfp*-mreB fusion (Hu *et al.*, 2007). In *Anabaena* WT, we observed GFP-MreB
311 filaments throughout the cells without any directional preferences and sometimes forming local
312 foci (Fig. 6A). Even though GFP-MreB filaments were present in the Δ*zicK*Δ*zacK* mutant strain
313 (Fig. 6A inlay), we only detected those filaments in non-rounded cells that seemingly had a
314 WT-like phenotype (Fig 6A), accounting for 24% of counted cells (245 of 1040 cells counted),
315 whereas in rounded/swollen cells of zigzagged trichomes, the GFP-MreB signals were
316 restricted to the cell poles (Fig. 6A), accounting for 76% of counted cells (795 of 1040 counted
317 cells). To further investigate the potential effect of *zicK* and *zacK* deletion on MreB and hence
318 elongasome function, we stained sites of active cell wall biosynthesis using a fluorescent
319 vancomycin derivate (Van-FL; (Daniel and Errington, 2003)). The staining pattern between the
320 WT and the Δ*zicK*Δ*zacK* mutant was indistinguishable but the fluorescence intensity levels
321 were slightly decreased in the Δ*zicK*Δ*zacK* mutant (Supplementary Fig. 9B,C). Nonetheless,

this is likely accounted for by the reduced growth rate of the Δ*zicK*Δ*zacK* mutant (Fig. 4D and general observation on growth plates).

Considering the interaction of ZicK/ZacK with ParA, we further tested for a function of ZicK and ZacK in DNA placement and compared the DNA distribution in the WT and the Δ*zicK*Δ*zacK* mutant as measured by distribution of 4′,6-Diamidin-2-phenylindol (DAPI) staining intensity (Fig. 6B,C). For that, we calculated the width of the DAPI focal area as the range of DAPI staining around the maximum intensity focus (±10 grey intensity in arbitrary units). This revealed that the staining focal area size was significantly different among the WT and the Δ*zicK*Δ*zacK* mutant. The DAPI signal observed in the Δ*zicK*Δ*zacK* mutant appears more condensed, and indeed, the Δ*zicK*Δ*zacK* mutant focal DAPI area was smaller than the WT (Fig. 6C). Unlike the WT, DAPI signals in the Δ*zicK*Δ*zacK* mutant was also observed between two neighbouring cells (Fig. 6B). Overall our results suggest the involvement of ZicK/ZacK in DNA distribution and segregation in dividing cells.

Discussion

Here we provide evidence for the capacity of two *Anabaena* CCRPs, which we termed ZicK and ZacK, to form polymers *in vitro* and *in vivo*. While the previously described prokaryotic filament-forming CCRPs formed homopolymers (Ausmees *et al.*, 2003; Yang *et al.*, 2004; Bagchi *et al.*, 2008; Specht *et al.*, 2011), ZicK and ZacK exclusively assembled into a heteropolymer *in vitro* and *in vivo*, thus revealing a new property of bacterial CCRPs. The inherent heteropolymerization tendency of ZicK and ZacK was confirmed in a heterologous and evolutionary distant *E. coli* system, which was previously used to investigate other known CCRPs such as Scc from *Leptospira biflexa* (England *et al.*, 2005) or Crescentin (Ingerson-Mahar *et al.*, 2010). Although heteropolymerization has previously been described for prokaryotic cytoskeletal proteins, none of those polymerization pairs both belonged to the group of CCRPs. BacA and BacB, members of the widely conserved class of bactofilins, both independently polymerize into filaments *in vitro*, co-localize *in vivo* in *C. crescentus* and interact directly with each other as indicated by co-immunoprecipitation analysis (Kühn *et al.*, 2010).

Unlike CCRPs, whose self-interaction is based on the high degree of CC domains, in bactofilins, the DUF583 domain is proposed to mediate protein polymerization (Kühn *et al.*, 2010). Despite compelling evidence for co-assembly and shared functional properties, heteropolymerization of BacA and BacB hasn't been studied *in vitro*. Another interesting pair of potential co-polymerizing cytoskeletal proteins that both independently assemble into homopolymers but also co-align *in vivo* and affect each other's properties are Crescentin and the CtpS enzyme from *C. crescentus* (Ingerson-Mahar *et al.*, 2010). Although, again, the co-assembly *in vitro* is not reported in the literature.

Despite the numerous independently confirmed heteropolymerization properties of ZicK and ZacK, we note, however, that the results from our *in vivo* experiments are based on artificial expression of the two CCRPs. We hypothesize that the absence of a ZicK/ZacK heteropolymer in strains expressing ZicK-GFP or ZacK-GFP alone (with the WT *zicK* and *zacK* alleles still present) may be due to a dosage-dependent effect, where the presence of unequal concentration of ZicK or ZacK in the cell leads to protein aggregates. Our observation of ZicK-GFP or ZacK-GFP aggregates when they were expressed alone in the Δ*zicK*Δ*zacK* mutant strain supports the dosage effect hypothesis. Also, in our *in vitro* polymerization assay, ZicK and ZacK only formed clear and distinct filament-like structures when both proteins are present in equal concentrations. Nonetheless, co-expressed of ZicK-eCFP and ZacK-GFP were not able to complement the Δ*zicK*Δ*zacK* mutant. Attempts to express both proteins fused to a fluorophore from the native promoter remained unsuccessful, possibly a result of the close genomic proximity. Furthermore, the genomic neighbourhood of *zicK* and *zacK* suggests that the ZicK/ZacK heteropolymer formation could be relying on co-translational assembly (e.g., as observed for LuxA/LuxB (Shieh *et al.*, 2015)). Co-translational assembly of natively present ZicK and ZacK would lead to an efficient binding of the two subunits such that the additional expression of one unit only in excess (*i.e.*, ZicK-GFP or ZacK-GFP alone) would lead to the formation of aggregates. As such, it remains to be elucidated to what extent the ZicK/ZacK heteropolymer exists in *Anabaena*. Although, we could not identify any protein filaments in our ultrathin sections from *Anabaena* WT, other studies have previously described filamentous

377 strings and even longitudinal cell-spanning polymers in multicellular *Anabaena* and *Nostoc*
378 strains (Jensen and Ayala, 1980; Bermudes *et al.*, 1994). Despite compelling evidence for the
379 existence of a cyanobacterial Z-ring structure during cell division (Sakr *et al.*, 2006b; Sakr *et*
380 *al.*, 2006a; Ramos-León *et al.*, 2015; MacCready *et al.*, 2017; Corrales-Guerrero *et al.*, 2018;
381 Camargo *et al.*, 2019), no Z-ring ultrastructures have yet been identified and consequently, the
382 absence of longitudinal ZicK/ZacK filaments in ultrathin sections does not rule out that they
383 exist but could rather indicate that they could not be visualized yet.

384 Our results indicate that ZicK and ZacK are associated with the elongasome (through
385 their interaction with MreB) and proteins in the septal cell wall (through the interaction with
386 SepJ and SepI) and affect cellular DNA placement (Fig. 7). A function of ZicK/ZacK in
387 chromosome segregation, would be in concert with the identified interaction of ZicK with ParA,
388 this, however, remains to be elucidated as it could also be an indirect consequence of the
389 swollen/rounded cell shape in the Δ*zick*Δ*zack* mutant. Nonetheless, so far no chromosome
390 partitioning system has yet been identified in multicellular cyanobacteria (Hu *et al.*, 2007). In
391 *E. coli*, *B. subtilis* and *C. crescentus*, MreB functions in chromosome segregation while deletion
392 of *mreB* did not affect chromosome segregation in *Anabaena* but induced a swollen cell
393 phenotype (Hu *et al.*, 2007), similar to the Δ*zick*Δ*zack* mutant. Consequently, MreB and
394 ZicK/ZacK likely share functional properties but are not exclusively involved in the same
395 cellular processes. Swollen cell morphotypes were also described for *Anabaena* or
396 *Synechocystis* mutants lacking penicillin binding proteins (PBPs), which are enzymes that are
397 directly involved in cell wall biogenesis through the modification of the PG layer (Lázaro *et al.*,
398 2001; Leganés *et al.*, 2005; Burnat *et al.*, 2014). This presumed link of ZicK/ZacK to the actin-
399 like MreB cytoskeleton and the PG biogenesis apparatus is also indicated by the altered
400 localization of GFP-MreB and the decreased PG staining intensity in the Δ*zicK*Δ*zacK* mutant
401 strain. Consequently, ZicK and ZacK might indirectly act to positively regulate PG biogenesis,
402 although, we cannot exclude that the reduced staining intensity in the Δ*zicK*Δ*zacK* mutant
403 simply reflects the slower growth rate of this strain. An interaction or involvement of prokaryotic
404 filament-forming CCRPs with MreB and PG synthesis were previously observed in other

bacteria. Examples are the gliding motility in *Myxococcus xanthus,* where a multiprotein complex, including the filament-forming CCRP AglZ and MreB, were found to coordinate type A-motility (Schumacher and Søgaard-Andersen, 2017). Similarly, the curved morphotype of *C. crescentus* is induced by Crescentin, which functionally associates with MreB and likely modulates PG biogenesis by exuding local mechanical forces to the cell membrane (Charbon *et al.*, 2009; Lin and Thanbichler, 2013). Other aspects like a decreased cell envelope permeability of the Δ*zicK*Δ*zacK* mutant are also conceivable, although we did not detect any cell wall defects in the Δ*zicK*Δ*zacK* mutant. MreB and the elongasome are the main determinants of the PG exoskeleton, which provides the cell with structural integrity and resistance to turgor pressure (Typas *et al.*, 2012). The lack of liquid growth of the Δ*zicK*Δ*zacK* mutant would also argue for a defect in the resistance to turgor pressure.

Together with the cell shape-determining protein MreB, ZicK and ZacK could possibly contribute to normal cell shape and relay trichome shape-stabilizing properties to neighbouring cells in the trichome by means of their association with the filament stabilizing protein SepJ (Fig. 7). As such, they are important for maintaining the linear *Anabaena* trichome phenotype. ZicK and ZacK polymers might constitute stabilizing platforms or scaffolds for other proteinaceous structures, similarly to the stabilizing function of the eukaryotic cytoskeleton for cell-cell contacts (*i.e.*, desmosomes). Furthermore, ZicK shares *in silico* predicted structural similarities with the spectrin repeats of plectin, a well-described eukaryotic cytolinker protein. Plectin link the three eukaryotic cytoskeletal systems (actin filaments, microtubules and IFs), thereby contributing to the resistance to deformation of vertebrate cells (Alberts *et al.*, 2014). They stabilize desmosomes and are hence directly involved in cell-cell contact integrity (Leung *et al.*, 2002). An analogous cytolinker function of ZicK could explain why ZacK alone did not form properly folded protein filaments on its own and suggests that ZacK requires ZicK as the linking protein for polymerization. As plectin not only stabilizes but also dynamically disassembles IF protein filaments (*i.e.*, vimentin) in a concentration-dependent manner (Birchler *et al.*, 2001), this would further support a dosage-dependent effect of ZicK and ZacK for heteropolymerization.

The conserved combination of ZicK and ZacK in heterocystous cyanobacteria that form linear trichomes (Fig. 1C, Supplementary File 2) highlights a potential function of ZicK and ZacK for the maintenance of the linear trichome. The Δ*zicK*Δ*zacK* mutant had a zigzagged phenotype and was unable to grow in liquid culture. We hypothesize that the loss of trichome linear shape led to an increase in accessible surface for the acting mechanical forces in liquid (Persat *et al.*, 2015), including fluid shear stress (Park *et al.*, 2011), ultimately resulting in forces that cannot be endured by the abnormal mutant trichomes. The loss of ZicK and/or ZacK in heterocystous cyanobacteria species that are in symbiosis (e.g., *N. azollae*) or form true-branching or multiseriate filaments (e.g., *Fischerella* or *Chlorogloeopsis*, respectively) may suggest that these species are less sensitive to mechanical stress (i.e., due to their interaction with the host or complex filament formation). The key hallmarks of permanent bacterial multicellularity are morphological differentiation and a well-defined and reproducible shape, termed patterned multicellularity (Claessen *et al.*, 2014). Besides the highly reproducible cell division, proliferation and cell differentiation in sporulating actinomycetes (Flärdh *et al.*, 2012), the reproducible linear trichomes in filamentous cyanobacteria are considered a major contributor to the cyanobacterial patterned multicellularity (Claessen *et al.*, 2014; Herrero *et al.*, 2016), manifesting a selective advantage to biotic and abiotic environmental factors (Young, 2006; Singh and Montgomery, 2011). Our results indicate that ZicK and ZacK serve as regulators of the typical linear *Anabaena* trichome and as such as regulators of *Anabaena* patterned multicellularity. The evolution of patterned multicellularity is considered an important step towards a sustainable division of labour and the development of cell differentiation (Claessen *et al.*, 2014). Our study provides initial evidence for a role of two heteropolymer-forming CCRPs in the evolution and maintenance of cyanobacterial multicellular forms.

Acknowledgments

We thank Myriam Barz, Katrin Schumann, Lisa-Marie Philipp, Lisa Stuckenschneider and Claudia Menzel for their assistance in the experimental work and Andreas Tholey for help with the mass spectrometry analysis. FRAP experiments were performed at the Facility for Imaging

by Light Microscopy (FILM) at Imperial College London. This study was supported by the German science foundation (DFG) (Grant No. STU513/2-1) and a Fondecyt Grant (Grant No. 11170842), both awarded to KS. IM was supported by German science foundation (DFG) (Grant SFB766). DJN was supported by the BBSRC as part of the joint NSF Ideas Lab grant on 'Nitrogen: improving on nature' (Grant No. BB/L011506/1).

Author contribution

BLS and KS designed the study. BLS established and performed the experimental work with contributions from MLT and JW. CW and TD performed comparative genomics analysis. DJN performed FRAP assays and IM carried out ultratstructure analyses. AOH and AT analysed protein samples by mass spectrometry. BLS, TD and KS drafted the manuscript with contributions from all co-authors.

Competing interests

The authors declare no competing interests.

Data availability

All data generated or analysed during this study are included in this published article (and its supplementary files).

Material and methods

Bacterial strains and growth conditions

Anabaena sp. PCC 7120 was obtained from the Pasteur Culture Collection (PCC) of cyanobacteria (France). Cells were grown photoautotrophically in BG11 or without combined nitrogen ($BG11_0$) at constant light with a light intensity of 30 µmol m^{-2} s^{-1} in liquid culture or on agar plates (1.5% w/v agar). When appropriate, 5 µg ml^{-1} spectinomycin (Sp), 5 µg ml^{-1} streptomycin (Sm) or 30 µg ml^{-1} neomycin (Nm) was added to strains carrying respective plasmids or chromosomal insertions. In some cases, basal copper-regulated *petE*-driven expression of gene candidates in *Anabaena* cells was lethal or growth inhibiting, therefore these strains were grown in BG11 without copper and protein expression was later induced by the addition of $CuSO_4$ at indicated concentrations to the culture. *E. coli* strains DH5α, DH5αMCR, XL1-blue and HB101 were used for cloning and conjugation by triparental mating. BTH101 was used for BACTH system and BL21 (DE3) was used for expression of His_6-tagged proteins in *E. coli*. All *E. coli* strains were grown in LB medium containing the appropriate antibiotics at standard concentrations. Supplementary Tables 1-4 list all used bacterial strains, plasmids and oligonucleotides.

Prediction of coiled-coil-rich proteins

Genome sequence of *Anabaena* (GCA_000009705.1) was analysed by the COILS algorithm (Lupas *et al.*, 1991) as previously described (Bagchi *et al.*, 2008). The algorithm was run with a window width of 21 and the cut-off for amino acids in coiled-coil conformation was set to ≥80 amino acid residues. The resulting set of protein candidates was further manually examined with online available bioinformatic tools, including NCBI Conserved Domain Search (Boratyn *et al.*, 2012), NCBI BLAST (Altschul *et al.*, 1990), TMHMM (Sonnhammer *et al.*, 1998) and I-TASSER (Zhang, 2009). Protein candidates exhibiting BLAST hits involved in cytoskeletal processes or similar domain architectures as known IF and IF-like proteins like Crescentin, FilP, vimentin, desmin or keratin were selected, and enzymatic proteins as well as proteins predicted to be involved in other cellular processes were excluded.

Distribution of homologs in cyanobacteria

Homologs to the *Anabaena* proteins were extracted from pre-calculated cyanobacterial protein families (Springstein *et al.*, 2020b). Conserved syntenic blocks (*i.e.*, gene order) were identified using CSBFinder-S (Svetlitsky *et al.*, 2020).

RNA isolation and cDNA synthesis

RNA from *Anabaena* WT was isolated using the Direct-zol™ RNA MiniPrep Kit (Zymo Research) according to the manufacturer's instructions. RNA was isolated in technical triplicates from 10 ml cultures. Isolated RNA was treated with DNA-free™ Kit (2 units rDNAs/reaction; Thermo Fischer Scientific) and 200 ng RNA was reverse transcribed using the qScript™ cDNA Synthesis Kit (Quanta Biosciences). RT-PCR of cDNA samples for *rnpB*, *zicK*, *zacK* and *zicK*+*zacK* was performed using primer pairs #1/#2, #3/#4, #5/#6 and #3/#8, respectively.

Transformation

Anabaena was transformed by triparental mating as previously described (Ungerer and Pakrasi, 2016). Briefly, 100 µl of overnight cultures of DH5α carrying the conjugal plasmid pRL443 and DH5αMCR carrying the cargo plasmid and the helper plasmid pRL623, encoding for three methylases, were mixed with 200 µl *Anabaena* culture (for transformation into the Δ*zick*ΔzacK mutant, cells were scraped from the plate and resuspended in 200 µl BG11). This mixture was directly applied onto sterilized nitrocellulose membranes (Amersham Protran 0.45 NC) placed on top of BG11 plates supplemented with 5% (v/v) LB medium. Cells were incubated in the dark at 30 °C for 6-8 h with subsequent transfer of the membranes to BG11 plates and plates were placed under standard growth conditions. After 24 h, membranes were transferred to BG11 plates supplemented with appropriate antibiotics.

Plasmid construction

Ectopic expression of *Anabaena* protein candidates was achieved from a self-replicating plasmid (pRL25C (Wolk *et al.*, 1988)) under the control of the copper-inducible *petE* promoter (P_{petE}) or the native promoter (predicted by BPROM (Solovyev and Salamov, 2011)) of the respective gene. All constructs were verified by Sanger sequencing (Eurofins Genomics). Plasmids were created using standard restriction enzyme-based techniques or Gibson assembly. Information about precise plasmid construction strategies are available from the authors upon request.

Anabaena mutant strain construction

The Δ*zick*ΔzacK mutant strain was generated using the pRL278-based double homologous recombination system employing the conditionally lethal *sacB* gene (Cai and Wolk, 1990). For this, 1500 bp upstream and downstream of *zick-zacK were* generated by PCR from *Anabaena* gDNA. Upstream region of *zicK* was amplified using primers #97/#98 and downstream region of *zacK* was amplified using primers #99/#100. The respective upstream and downstream homology regions flanking the CS.3 cassette (amplified with primer #95/#96 from pCSEL24) were then inserted into PCR-amplified pRL278 (using primer #93/#94) by Gibson assembly, yielding pTHS166. *Anabaena* transformed with pTHS166 plasmids was subjected to several rounds of re-streaking on new plates (about 5-8 rounds). To test for fully segregated clones, colony PCRs were performed. For this, *Anabaena* cells were resuspended in 10 µl sterile H_2O of which 1 µl was used for standard PCR with internal *zicK* and *zacK* gene primers #3/#6. Correct placement of the CS.3 cassette was then further confirmed using CS.3 cassette primers with binding sites outside of the 5' and 3' flanks used for homologous recombination (primers #95/#102 and #101/#96).

Fluorescence microscopy

Bacterial strains grown in liquid culture were either directly applied to a microscope slide or previously immobilized on a 2% (w/v) low-melting agarose in PBS (10 mM Na_2HPO_4, 140 mM

NaCl, 2.7 mM KCl, 1.8 mM KH_2PO_4, pH 7.4) agarose pad and air dried before microscopic analysis. Epifluorescence was done using an Axio Imager.M2 light microscope (Carl Zeiss) equipped with Plan-Apochromat 63x/1.40 Oil M27 objective and the AxioCam MR R3 imaging device (Carl Zeiss). GFP, Alexa Fluor 488 and BODIPY™ FL Vancomycin (Van-FL) fluorescence was visualized using filter set 38 (Carl Zeiss; excitation: 470/40 nm band pass (BP) filter; emission: 525/50 nm BP). Chlorophyll auto-fluorescence was recorded using filter set 15 (Carl Zeiss; excitation: 546/12 nm BP; emission: 590 nm long pass). When applicable, cells were previously incubated in the dark at RT for about 5 min with 10 µg ml^{-1} DAPI (final concentration) to stain intracellular DNA. For visualization of DAPI fluorescence filter set 49 (Carl Zeiss; excitation: G 365 nm; emission: 455/50 nm) was employed. For confocal laser scanning microscopy, the LSM 880 Axio Imager 2 equipped with a C-Apochromat 63x/1.2 W Korr M27 objective and an Airyscan detector (Carl Zeiss) was used and visualization of GFP, eCFP and chlorophyll auto-fluorescence was done using Zen black smart setup settings.

Transmission electron microscopy

For ultra-structure analysis, *Anabaena* trichomes were fixed with 2.5% (v/v) glutaraldehyde, immobilized in 2% (w/v) agarose, treated with 2% (v/v) potassium permanganate and dehydrated through a graded ethanol series (Mohr *et al.*, 2010). The fixed cells were infiltrated by ethanol:EPON (2:1 to 1:2 ratio) and embedded in pure EPON. Ultrathin sections were prepared with a Leica UC6i Ultramicrotome, transferred to formvar coated copper grids (Science Services GmbH München) and post-stained with uranyl acetate and lead citrate (Fiedler *et al.*, 1998). Micrographs were recorded at a Philips Tecnai10 electron microscope at 80 kV.

Calcein labelling and fluorescence recovery after photobleaching (FRAP) experiments

For FRAP experiments, *Anabaena* WT and Δ*zick*Δ*zacK* mutant strain were grown on BG11 plates, resuspended in BG11 liquid media and washed three times in 1 ml BG11 (3,000 x *g*, 5 min). Cells were then resuspended in 0.5 ml BG11 and incubated with 10 µl calcein-AM (Cayman Chemical, 1 mg ml^{-1} in DMSO) for 1 h at 30 °C in the dark. To remove excess staining

579 solution the cells were washed four times with 1 ml BG11. Subsequently, the cells were spotted
580 on BG11 agar for visualization by confocal laser scanning microscopy (Leica TCS SP5; HCX
581 PL APO 63x 1.40-0.60 OIL CS). Calcein was excited at 488 nm and fluorescence emission
582 monitored in the range from 500 to 530 nm with a maximally opened pinhole (600 µm). FRAP
583 experiments were carried out by an automated routine as previously described (Mullineaux *et*
584 *al.*, 2008). After recording an initial image, selected cells were bleached by increasing the laser
585 intensity by a factor of 5 for two subsequent scans and the fluorescence recovery followed in
586 0.5 s intervals for 30 s was recorded using the Leica LAS X software. Exchange coefficients
587 (*E*) were then calculated as previously described (Mullineaux *et al.*, 2008; Nieves-Morión *et*
588 *al.*, 2017).

589 *BODIPY™ FL Vancomycin (Van-FL) staining*

590 Van-FL staining of strains grown on BG11 plates was essentially performed as described
591 previously (Lehner *et al.*, 2013; Rudolf *et al.*, 2015). Briefly, cells were resuspended in BG11
592 medium, washed once in BG11 by centrifugation (6500 x *g*, 4 min, RT) and incubated with 5
593 µg ml^{-1} Van-FL (dissolved in methanol; Thermo Fischer Scientific). Cells were incubated in the
594 dark for 1 hour at 30 °C, washed three times with BG11 and immobilized on an agarose pad.
595 Van-FL fluorescence signals were then visualized using epifluorescence microscopy with an
596 excitation time of 130 ms. Arithmetic mean fluorescence intensities were recorded from the
597 septa between two cells with a measured area of 3.52 $µm^2$ using the histogram option of the
598 Zen blue 2.3 software (Carl Zeiss).

599 *Alcian blue staining*

600 *Anabaena* WT and Δ*zicK*Δ*zicK* cells were grown on $BG11_0$ plates, re-suspended in $BG11_0$
601 liquid medium and stained with 0.05% (w/v) alcian blue (final concentration). Polysaccharide
602 staining of cells immobilized on an agarose pad was observed with an Axiocam ERc 5s color
603 camera (Carl Zeiss).

Data analysis

Cell volume and roundness were determined using the imaging software ImageJ (Schneider *et al.*, 2012), a perfect circle is defined to have a roundness of 1. Cell volume was calculated based on the assumption of an elliptic cell shape of *Anabaena* cells using the Major Axis and Minor Axis values given by ImageJ and the formula for the volume of an ellipsoid

$$\left(V = \frac{4}{3}\pi abc\right) = V = \frac{4}{3}\pi\left(\left(\frac{Major\ Axis}{2}\right)^2 \frac{Minor\ Axis}{2}\right)$$

Distribution of DAPI fluorescence signal intensity was analysed in ImageJ with the Plot Profile option along 151 single cells with the rectangle tool. The resulting grey values were arranged according to the maximum intensity focus and the width of the DAPI focal area was calculated as the range of DAPI staining around the maximum (±10 grey value in arbitrary units). Statistical tests were performed with MatLab© (MathWorks) or GraphPad Prism v.8.

Bacterial two-hybrid and beta galactosidase assays

Chemically competent *E. coli* BTH101 cells were co-transformed with 5 ng of plasmids carrying the respective T18 and T25 translational fusion constructs, plated onto LB plates supplemented with 200 µg ml^{-1} X-gal, 0.5 mM IPTG, Amp, Km and grown at 30°C for 24-36 h. Interactions were quantified by beta-galactosidase assays from three independent colonies. For this aim, cultures were grown for two days at 20 °C in LB Amp, Km, 0.5 mM IPTG and beta-galactosidase activity was recorded as described in the manufacturer's instructions (Euromedex; BACTH System Kit Bacterial Adenylate Cyclase Two-Hybrid System Kit) in a 96 well plate format as previously described (Karimova *et al.*, 2012).

GFP-fragment reassembly assay

Chemically competent *E. coli* BL21 (DE3) were co-transformed with indicated plasmid combinations, plated on LB Amp, Km and grown over night at 37 °C. Liquid overnight cultures of single colonies of the respective plasmid-bearing *E. coli* strains were then diluted 1:40 in the same medium the following day. Cells were grown for 2 h at 37 °C, briefly acclimated to 20 °C

for 10 min and protein expression was induced with 0.05 mM IPTG and 0.2% (w/v) L-arabinose. Pictures of induced cultures grown at 20 °C were taken 48 h after induction.

Co-immunoprecipitation

About 20-30 ml of the respective *Anabaena* cultures were pelleted by centrifugation (4800 x *g*, 10 min, RT), cells were washed twice by centrifugation (4800 x *g*, 10 min, RT) with 40 ml PBS and then resuspended in 1 ml lysis buffer (PBS-N: PBS with 1% (v/v) NP-40) supplemented with protease inhibitor cocktail (PIC; cOmplete™, EDTA-free Protease Inhibitor Cocktail, Sigma-Aldrich). Cells were lysed using the VK05 lysis kit (Bertin) in a Precellys® 24 homogenizer (3 strokes for 30 s at 6500 rpm) and cell debris was pelleted by centrifugation (30 min, 21,100 x *g*, 4 °C). 50 µl µMACS anti-GFP MicroBeads (Miltenyi Biotec) were added to the resulting cell-free supernatant and incubated for 1 h at 4 °C with mild rotation. Subsequently, the sample was loaded onto µColumns (Miltenyl Biotec), washed two times with 1 ml lysis buffer and eluted in 50 µl Elution Buffer (50 mM Tris HCl pH 6.8, 50 mM DTT, 1% (w/v) SDS, 1 mM EDTA, 0.005% (w/v) bromophenol blue, 10% (v/v) glycerol; Miltenyl Biotec). Samples were stored at -80 °C until further use.

Mass spectrometry

Mass spectrometry of co-precipitated proteins was performed as previously described (Springstein *et al.*, 2020a).

Immunofluorescence

Immunolocalization of FtsZ in *Anabaena* WT and Δ*zicK*Δ*zacK* mutant was essentially performed as previously described (Ramos-León *et al.*, 2015). For this, strains were scraped off from growth plates (BG11 and $BG11_0$ plates), resuspended in a small volume of distilled water and air-dried on Polysine® adhesion slides (Menzel) at RT followed by fixation and permeabilization with 70% ethanol for 30 min at -20 °C. Cells were allowed to air dry for 30 min at RT and then washed two times with PBST (PBS supplemented with 0.1% (v/v) Tween-20) for 2 min. Unspecific binding sites were blocked for 30 min at RT with blocking buffer (1x

Roti®-ImmunoBlock in PBST; Carl Roth) and afterwards rabbit anti-FtsZ (Agrisera; raised against *Anabaena* FtsZ; 1:150 diluted) antibody in blocking buffer was added to the cells and incubated for 1.5 h at RT in a self-made humidity chamber followed by five washing steps with PBST. 7.5 µg ml^{-1} (final concentration) Alexa Fluor 488-conjugated goat anti-rabbit IgG (H+L) secondary antibody (Thermo Fischer Scientific) in blocking buffer was added to the cells and incubated for 1 h at RT in the dark in a self-made humidity chamber. Subsequently, cells were washed five times with PBST, air dried and mounted with ProLong™ Diamond Antifade Mountant (Thermo Fischer Scientific) overnight at 4 °C. Immunolocalization of FtsZ was then analysed by epifluorescence microscopy.

Spot assays

For spot assays, *Anabaena* WT and Δ*zicK*Δ*zacK* mutant strain were grown on BG11 growth plates, resuspended in BG11 liquid medium and adjusted to an OD_{750} of 0.4. Cells were then spotted in triplicates of 5 µl onto the respective growth plates containing either no additives (BG11 or $BG11_0$), 50 µg ml^{-1} Proteinase K or 100 µg ml^{-1} lysozyme in serial 1/10 dilutions and incubated under standard growth conditions until no further colonies arose in the highest dilution.

Protein purification and in vitro filamentation assays

For protein purification, *E. coli* BL21 (DE3) cells carrying His-tagged protein candidates were grown in overnight cultures at 37 °C and 250 rpm. The next day, overnight cultures were diluted 1:40 in the same medium and grown at 37 °C until they reached an OD_{600} of 0.5-0.6. Protein expression was induced with 0.5 mM IPTG for 3-4 h at 37 °C and 250 rpm. Afterwards, cell suspensions of 50 ml aliquots were harvested by centrifugation, washed once in PBS and stored at -80 °C until further use. For *in vitro* filamentation assays, cell pellets were resuspended in urea lysis buffer (ULB: 50 mM NaH_2PO_4, 300 mM NaCl, 25 mM imidazole, 6 M urea; pH 8.0) and lysed in a Precellys® 24 homogenizer (3x 6500 rpm for 30 s) using the 2 ml microorganism lysis kit (VK01; Bertin) or self-packed Precellys tubes with 0.1 mm glass beads. The resulting cell debris was pelleted by centrifugation at 21,000 x *g* (10 min, 4 °C) and

682 the supernatant was incubated with 1 ml HisPur™ Ni-NTA resin (Thermo Fischer Scientific)
683 for 1 h at 4°C in an overhead rotator. The resin was washed five times with 4x resin-bed
684 volumes ULB and eluted in urea elution buffer (UEB: ULB supplemented with 225 mM
685 imidazole). Total protein concentration was measured using the Qubit® 3.0 Fluorometer
686 (Thermo Fischer Scientific). Filament formation of purified proteins was induced by overnight
687 dialysis against polymerization buffer (PLB: 50 mM PIPES, 100 mM KCl, pH 7.0; HLB: 25 mM
688 HEPES, 150 mM NaCl, pH 7.4; or 25 mM HEPES pH 7.5) at 20 °C and 180 rpm with three
689 bath changes using a Slide-A-Lyzer™ MINI Dialysis Device (10K MWCO, 0.5 ml or 2 ml;
690 Thermo Fischer Scientific). Purified proteins were stained with an excess of NHS-Fluorescein
691 (dissolved in DMSO; Thermo Fischer Scientific) and *in vitro* filamentation was analysed by
692 epifluorescence microscopy. The NHS-Fluorescein dye was previously successfully used to
693 visualize *in vitro* FtsZ and CCRP protein filaments (Camberg *et al.*, 2009; Springstein *et al.*,
694 2020b). And we note that the His_6-tag did not impact the *in vitro* polymerization properties of
695 the CCRP FilP (Javadi *et al.*, 2019), confirming the applicability of our approach.

Figures

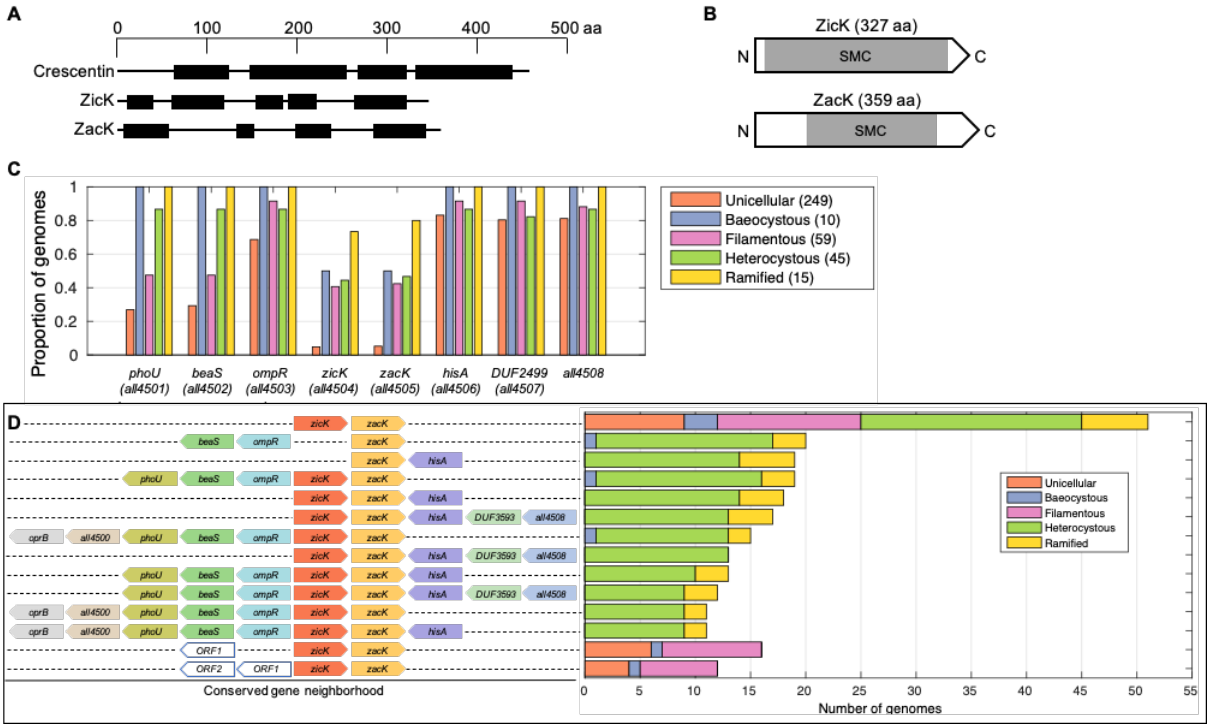

Fig. 1: Conservation of ZicK and Zack among cyanobacterial species and domain architecture

(**A**) Depiction of coiled-coil domains of ZicK and ZacK as identified by the COILS algorithm (Lupas *et al.*, 1991) with a window width of 21. As a comparison, Crescentin from *C. crescentus* is also included. The scale on top is given in amino acid residues (aa) and amino acid sequences in coiled-coil conformation are depicted by black bars, while non-coiled-coil sequences are represented by black lines. (**B**) Schematic depiction of the domain architecture of ZicK and ZacK. The SMC domains predicted for both proteins are depicted by grey bars. (**C**) The presence of homologs of ZicK/ZacK in cyanobacteria main types (total number of genomes in the analysis is shown in the legend). Note that the presence of ZicK/ZacK homologs in baeocystous cyanobacteria is in accordance with a recent suggestion of a multicellular ancestry of species in that group (Urrejola *et al.*, 2020). (**D**) Genomic neighbourhood of ZicK/ZacK in cyanobacterial genomes. Conserved syntenic blocks (CSBs; *i.e.*, conserved gene order) are shown on the left; the number of genomes where the same gene order has been identified is shown by a bar right of the conserved gene order. Genes with clear annotation or unique locus name are designated as ORF. Note that the CSBs are not mutually exclusive - *i.e.*, the longer CSBs where ZicK/ZacK are neighbours (and in the same orientation) include the ZicK/ZacK CSB (1st line on top). The 2nd line from the top shows the CSB in organisms where ZicK is absent. The two CSBs at the bottom reveal that the genomic neighbourhood of ZicK/ZacK in non-heterocystous cyanobacteria is different in comparison to heterocystous cyanobacteria.

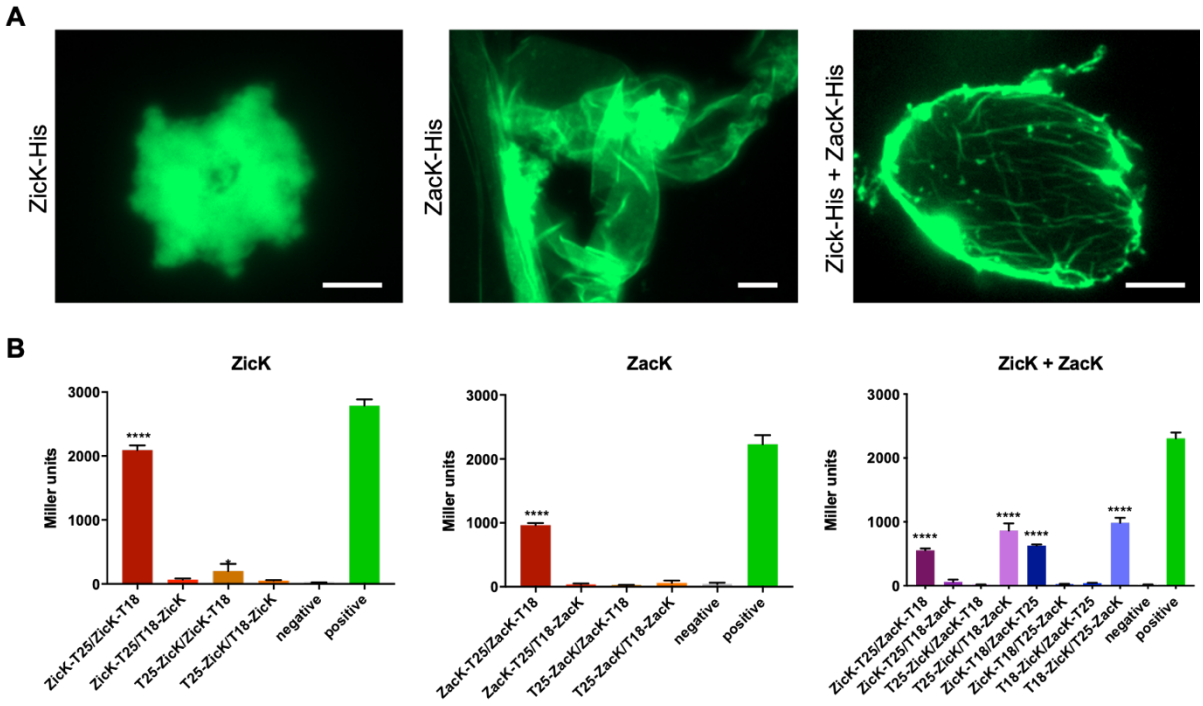

Fig. 2: ZicK and ZacK form heteropolymer filament-like structures and interact *in vivo*

(**A**) Epifluorescence micrographs of NHS-Fluorescein-stained *in vitro* structures formed by purified and renatured ZicK-His (1 mg ml^{-1}), ZacK-His (0.5 mg ml^{-1}) or co-renatured ZicK-His and ZacK-His (0.25 mg ml^{-1} each) in 25 mM HEPES, pH 7.4 (ZacK) or HLB (ZicK and co-renatured ZicK/ZacK) renaturation buffer. Note: although ZacK formed somewhat filamentous structures *in vitro*, the vast majority of ZacK clumped into aggregates, reminiscent of GroEL1.2 (Supplementary Fig 2). (**B**) BACTH assays of *E. coli* cells co-expressing indicated T25 and T18 translational fusions of all possible pair-wise combinations of ZicK and ZacK. *E. coli* cells were subjected to beta-galactosidase assay in triplicates from three independent colonies grown for 2 d at 20°C. Quantitative values are given in Miller units, and the mean results from three independent colonies are presented. Negative: N-terminal T25 fusion construct of the respective protein co-transformed with empty pUT18C. Positive: Zip/Zip control. Error bars indicate standard deviations (n = 3). Values indicated with asterisks are significantly different from the negative control. ****: $p < .0001$ (Student's t-test).

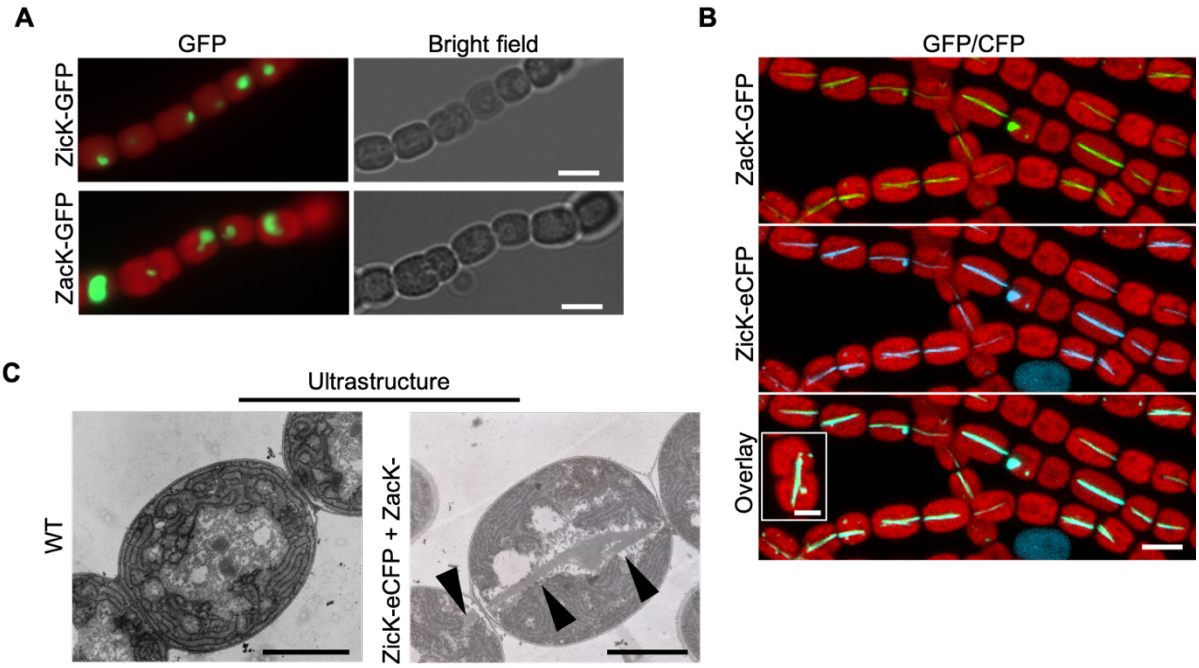

Fig. 3: ZicK and ZacK form a heteropolymer *in vivo*

(**A**,**B**) Merged GFP or eCFP-fluorescence and chlorophyll autofluorescence (red) and bright field micrographs of *Anabaena* WT cells expressing (**A**) ZicK-GFP, ZacK-GFP or (**B**) co-expressing ZicK-eCFP and ZacK-GFP from P_{petE}. (**B**) Inlay shows that ZicK/ZacK filaments only cross not yet fully divided cells. Scale bars: (A,B) 5 µm, (B inlay) 2.5 µm. (**C**) Electron micrographs of ultrathin sections of *Anabaena* WT and *Anabaena* cells co-expressing ZicK-eCFP and ZacK-GFP. Black arrows indicate electron-dense structures coinciding with the ZicK/ZacK heteropolymer observed in Fig. 4B. Scale bars: 1.6 µm.

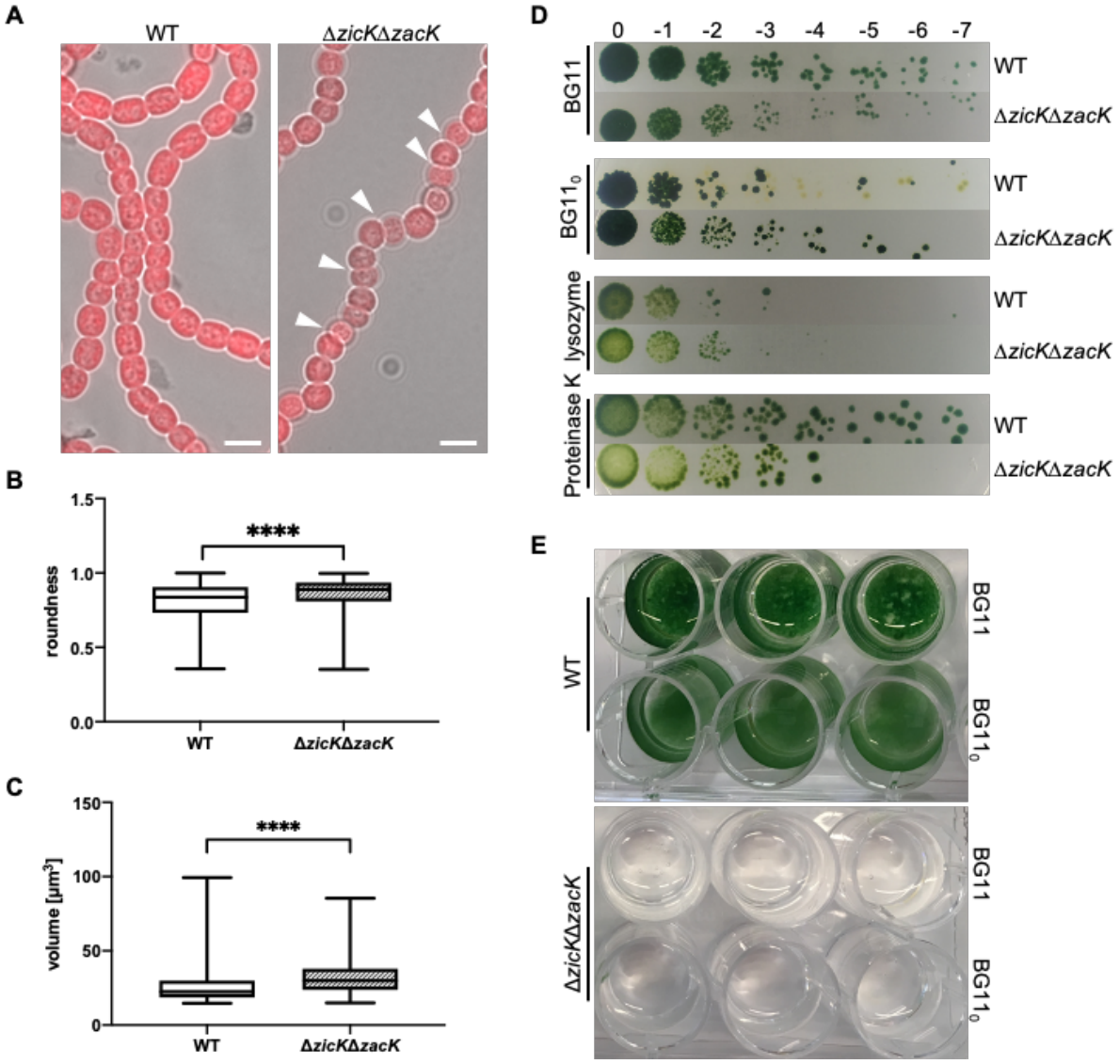

739

740 **Fig. 4: Deletion of *zicK* and *zacK alters trichome and cell shape as well as trichome viability***

741 (**A**) Merged chlorophyll autofluorescence and bright field micrographs of *Anabaena* WT and
742 Δ*zicK*Δ*zacK* mutant grown on BG11 plates. White triangles indicate zigzagged trichome growth.
743 Scale bars: 5 µm. (**B**) Cell roundness and (**C**) volume of *Anabaena* WT and Δ*zicK*Δ*zacK* mutant
744 measured with Fiji imaging software A perfect circle is defined as roundness of 1. Error bars indicate
745 standard deviations (*Anabaena* WT: n=537; Δ*zicK*Δ*zacK*: n=404). Values indicated with asterisks
746 are significantly different from the WT. ****: p < .0001 (Student's t-test). (**D**) *Anabaena* WT and
747 Δ*zicK*Δ*zacK* mutant were spotted onto BG11, BG11$_0$ or BG11 plates supplemented with lysozyme
748 or Proteinase K in triplicates of serial dilutions of factor 10 and grown until no further colonies arose
749 in the highest dilution (n=2). (**E**) *Anabaena* WT and Δ*zicK*Δ*zacK* mutant were grown on BG11
750 plates, transferred to liquid BG11 and BG11$_0$ medium and incubated for 12 d at standard growth
751 conditions without shaking.

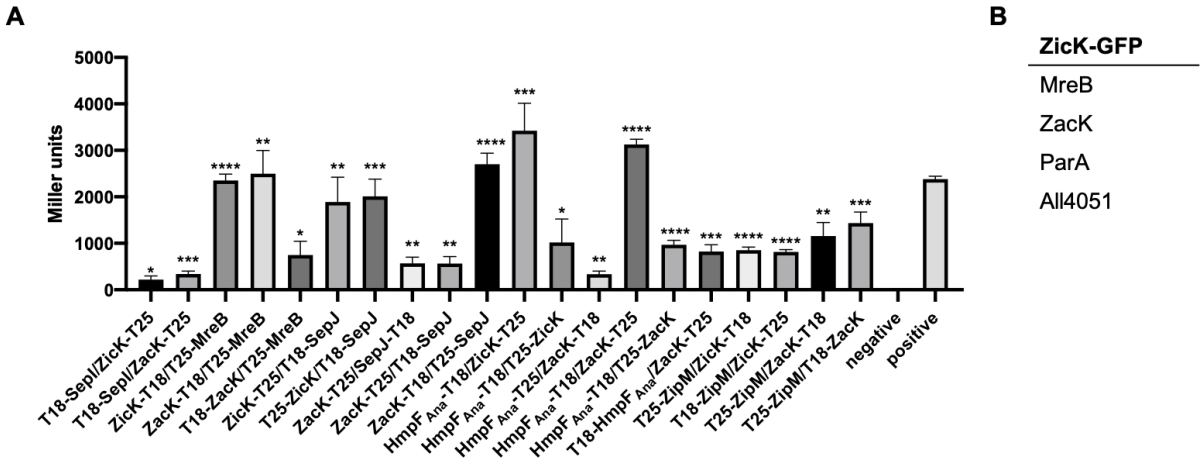

752

753 **Fig. 5: ZicK and ZacK interact with a multitude of *Anabaena* proteins involved in cell shape and**
754 **multicellularity**

755 (**A**) BACTH assays of *E. coli* cells co-expressing indicated T25 and T18 translational fusions of indicated
756 pair-wise combinations of ZicK, ZacK, SepI, MreB, SepJ, $HmpF_{Ana}$ and ZipM. Only translational fusion
757 combinations that resulted in a significant interaction between two analysed proteins are shown. All
758 other combinations were negative for interaction. Note that we used full-length proteins for all our
759 BACTH analysis, including SepJ, whose precise subcellular localization remains to be identified
760 (Ramos-León *et al.*, 2017; Springstein *et al.*, 2020a) but could be different in *E. coli* and *Anabaena*
761 (Springstein *et al.*, 2020a). Quantitative values are given in Miller units, and the mean results from three
762 independent colonies are presented. Negative: N-terminal T25 fusion construct of the respective protein
763 co-transformed with empty pUT18C. Positive: Zip/Zip control. Error bars indicate standard deviations
764 (n = 3). Values indicated with asterisks are significantly different from the negative control. *: $p < .05$,
765 **: $p < .005$, ***: $p < .0005$, ****: $p < .0001$ (Student's t-test). (**B**) Excerpt of the identified specific
766 interactors of ZicK-GFP. The full list is listed in Supplementary File 3.

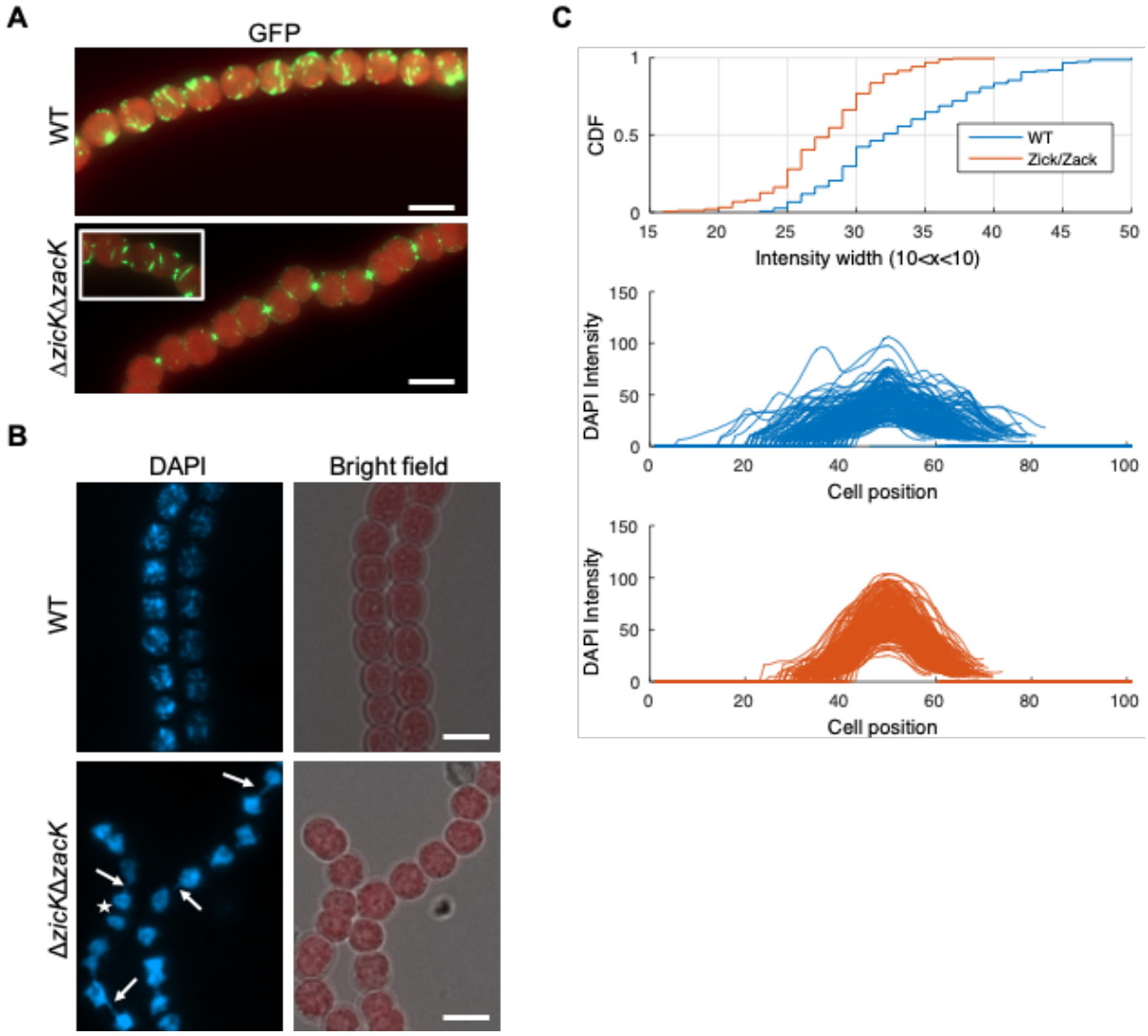

Fig. 6: Effect of *zicK* and *zacK* deletion on MreB localization and DNA distribution

(**A**) Merged GFP fluorescence and chlorophyll autofluorescence micrographs of *Anabaena* WT and Δ*zicK*Δ*zacK* mutant expressing GFP-MreB from P_{petE}. Cells were grown on BG11 plates. Scale bars: 5 µm. (**B**) DAPI fluorescence and merged bright field and chlorophyll autofluorescence micrographs of *Anabaena* WT and Δ*zicK*Δ*zacK* mutant on BG11 plates. White arrows indicate strings of DNA that seemingly traverse from one cell to the other. Notably, no such strings are observed in dividing cells (white star), suggesting that it is an effect that occurs after complete cell division. Although, we note that high resolution microscopy would be needed to fully resolve this observation. Scale bars: 5 µm. (**C**) Plot profile showing a cumulative distribution function (CDF) of the DAPI signal intensities of pixels (grey value) along *Anabaena* WT and Δ*zicK*Δ*zacK* mutant cells (n=151 for each strain) in arbitrary units (a.u.) and arranged to the respective peak maxima. The focal area size in the Δ*zicK*Δ*zacK* mutant was smaller in comparison to the *Anabaena* WT ($P=6.8x10^{-117}$, using Wilcoxon test). Notably, the comparison of cell lenght among the strains reveals a similar result: the Δ*zicK*Δ*zacK* mutant cell size was smaller in comparison to the *Anabaena* WT ($P=7.2x10^{-117}$, using Wilcoxon test). Consequently, we compared the area of the focal DAPI staining decided by the cell size among the strains. This, however, revealed that this ratio is not significantly different between the Δ*zicK*Δ*zacK* mutant and the *Anabaena* WT.

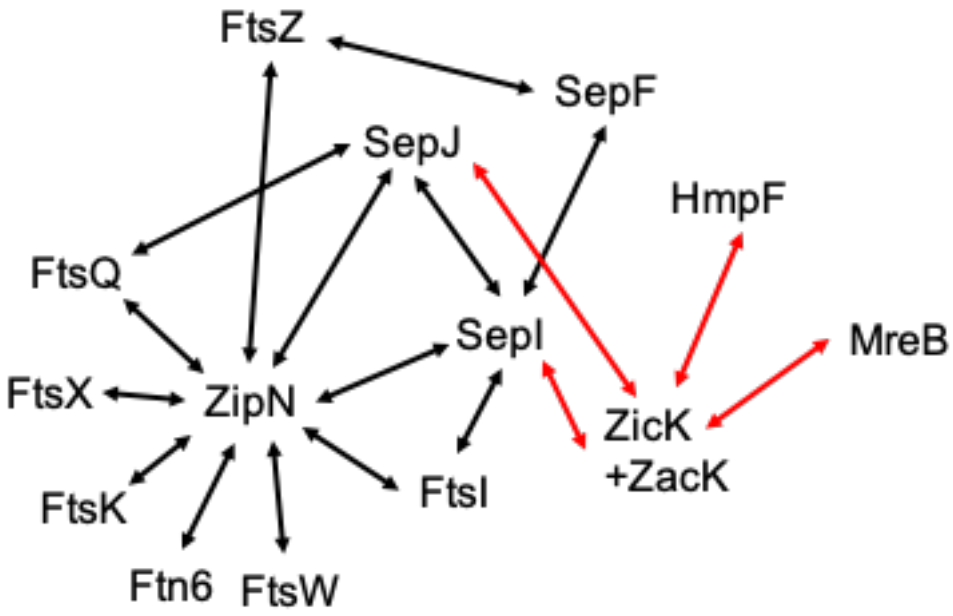

784

785 **Fig. 7: Interaction network of known divisome, elongasome and septal proteins in *Anabaena***

786 A model for a partial divisome, elongasome and septal junction network in *Anabaena* as deduced from
787 BACTH and co-IP analyses. Black arrows indicate interactions that have been previously described by
788 (Ramos-León *et al.*, 2015; Camargo *et al.*, 2019; Springstein *et al.*, 2020a). Red arrows indicate
789 interactions identified in the current analysis.

Supplementary Figures

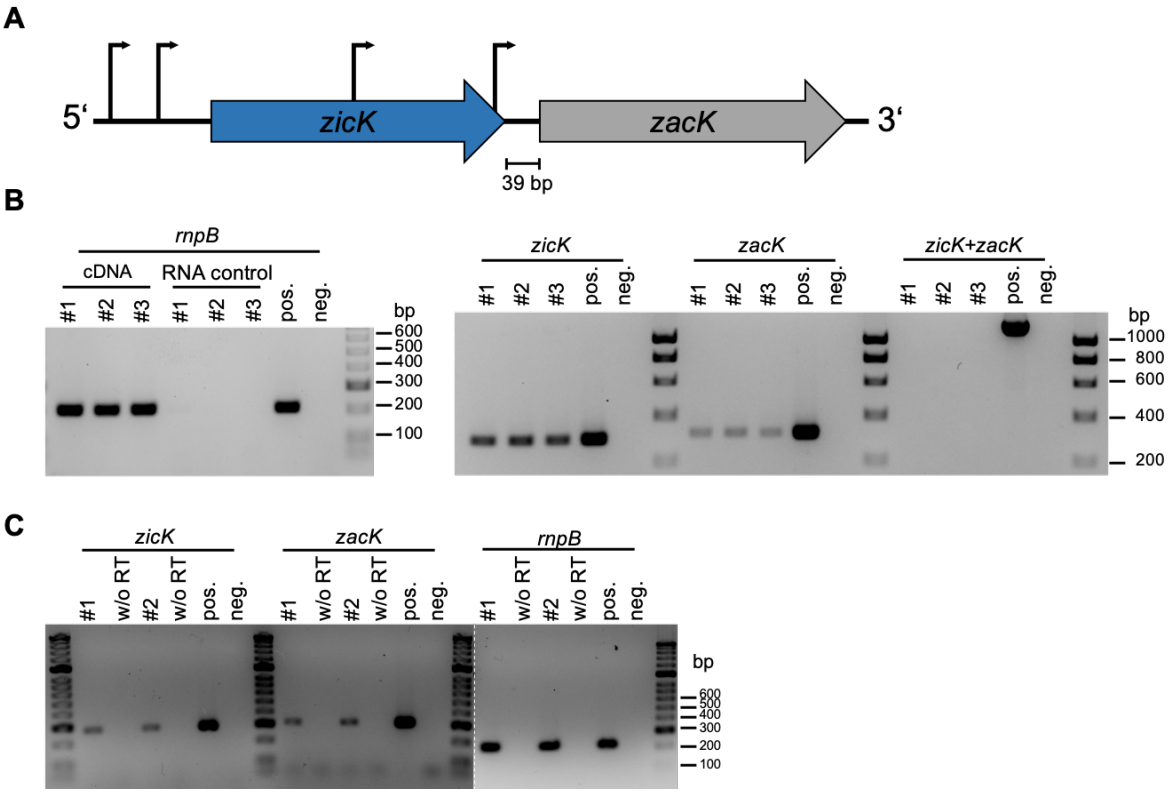

Supplementary Fig. 1: *zicK* and *zacK* are expressed at standard growth conditions

(**A**) Depiction of the genomic environment of *zicK* (blue) and *ZacK* (grey) within the *Anabaena* genome and their respective *in silico* predicted promoters depicted by black arrows (as predicted by BPROM (Solovyev and Salamov, 2011)). Promoters of *zicK* are predicted to reside 204 bp and 543 bp upstream of the open reading frame (ORF) and promoters of *zacK* are located 22 bp and 450 bp upstream of the ORF, thereby residing within the *zicK* ORF. (**B**,**C**) RT-PCR of whole cell RNA from *Anabaena* WT cultures grown in (**B**) BG11 or (**C**) $BG11_0$ liquid medium from (**B**) three or (**C**) two independent biological replicates. Gene transcripts were verified using internal gene primers (Supplementary Table 4). As negative control (neg), PCR reactions were performed with water instead of cDNA or RNA and as a positive control (pos) *Anabaena* gDNA was included. 100 ng cDNA was used for each RT-PCR reaction. Absence of residual genomic DNA in DNase I-treated samples was verified with (**B**) 100 ng DNase I-treated RNA (RNA control) or (**C**) 100 ng DNase I-treated RNA that was subjected to cDNA synthesis reaction lacking reverse transcriptase (w/o RT).

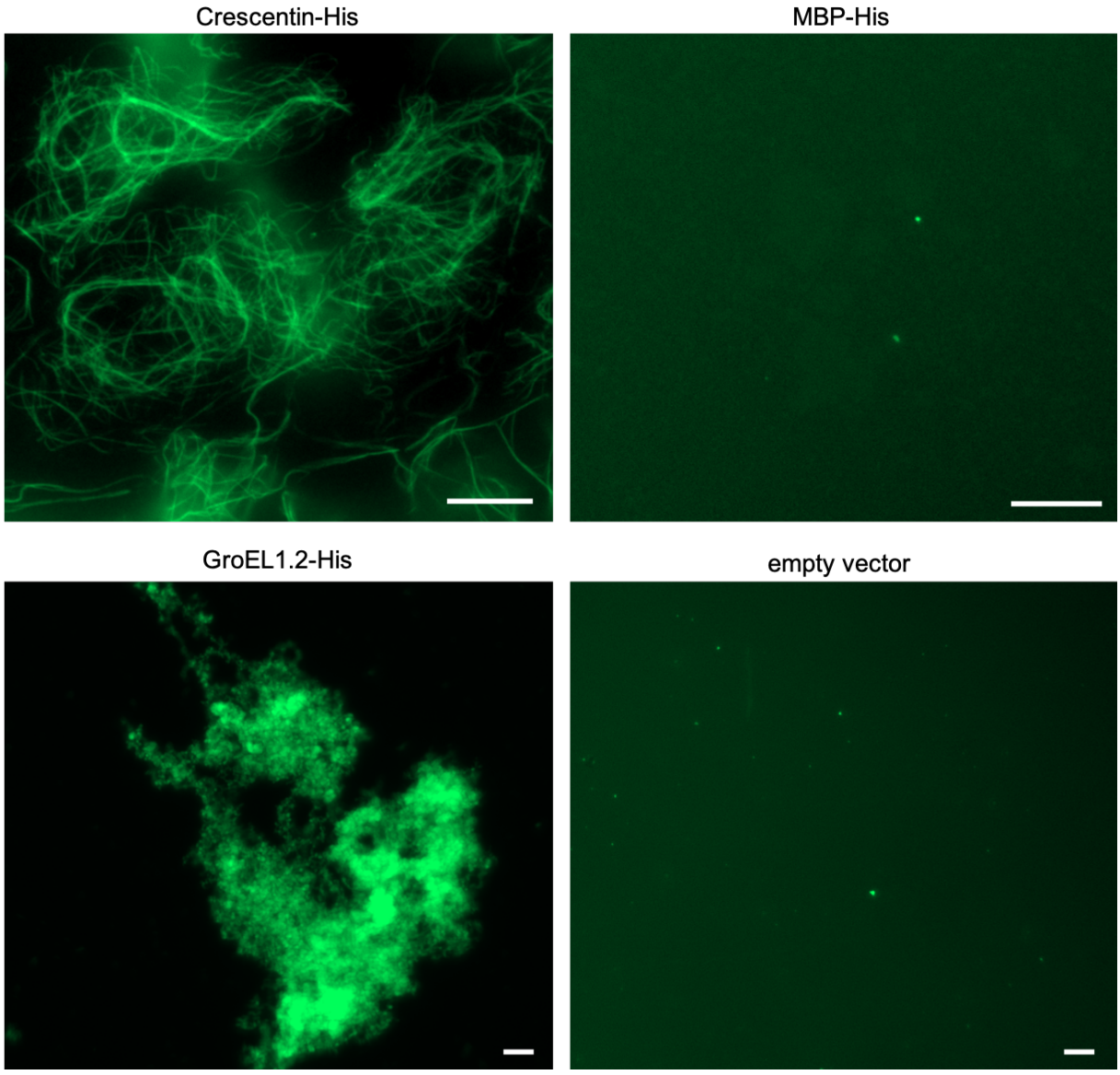

Supplementary Fig. 2: *In vitro* polymerization assay controls

NHS-fluorescein fluorescence micrographs of purified and renatured Crescentin-His, MBP-His and GroEL1.2 from *Chlorogloeopsis fritschii* PCC 6912 (0.5 mg ml^{-1} each) as well as purified cell-free extracts of *E. coli* BL21 (DE3) carrying empty vector (pET21a(+)) in HLB. While neither the cell-free extract containing empty vector nor the MBP protein formed any discernible structures *in vitro*, GroEL1.2 aggregates could be indicative for an uncontrolled oligomerization. We also observed similar clumps of protein aggregates from other *Anabaena* CCRPs that were negatively tested for *in vitro* polymerization. We therefore consider this *in vitro* behaviour a common property of putative oligomerizing proteins. Proteins and cell-free extracts (empty vector) were dialyzed in a stepwise urea-decreasing manner and stained with an excess of NHS-Fluorescein. Scale bars: 10 µm.

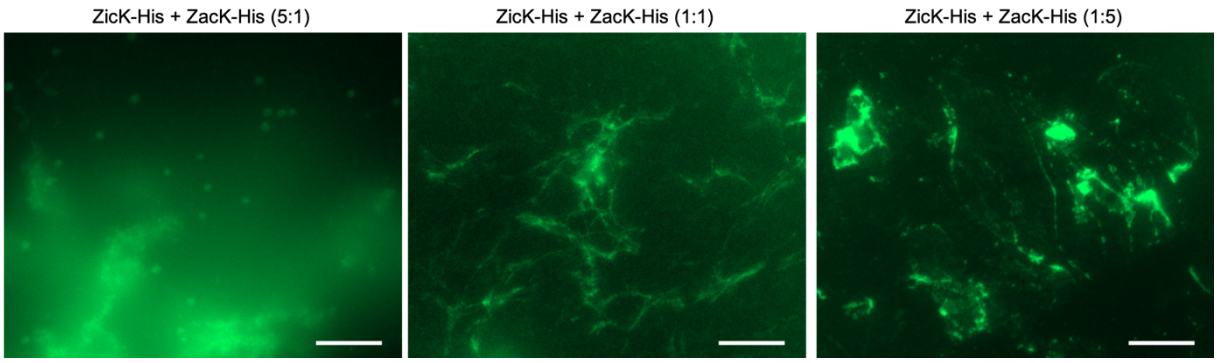

Supplementary Fig. 3: Co-polymerization of ZicK and ZacK is dosage-dependent

NHS-fluorescein micrographs of purified and co-renatured ZicK-His and ZacK-His in HLB renaturation buffer. ZicK-His and ZacK-His were combined in different ratios, either with a fivefold excess of ZicK-His (left image; corresponding to 0.25 mg ml^{-1} ZicK-His and 0.05 mg ml^{-1} ZacK-His), a fivefold excess of ZicK-His (right image; corresponding to 0.25 mg ml^{-1} ZacK-His and 0.05 mg ml^{-1} ZicK-His) or an equal concentration of ZicK-His and ZacK-His (central image; 0.25 mg ml^{-1} each). Proteins were dialyzed in a step-wise urea-decreasing manner and stained with an excess of NHS-Fluorescein. Fine heteropolymers only form when equal concentrations of ZicK-His and ZacK-His are present. In concert with the partial self-polymerization capacity of ZacK-His (Fig. 3A), certain filamentous structures are also detected in the ZacK-His excess samples. However, most protein still precipitated under those conditions. Scale bars: 10 µm.

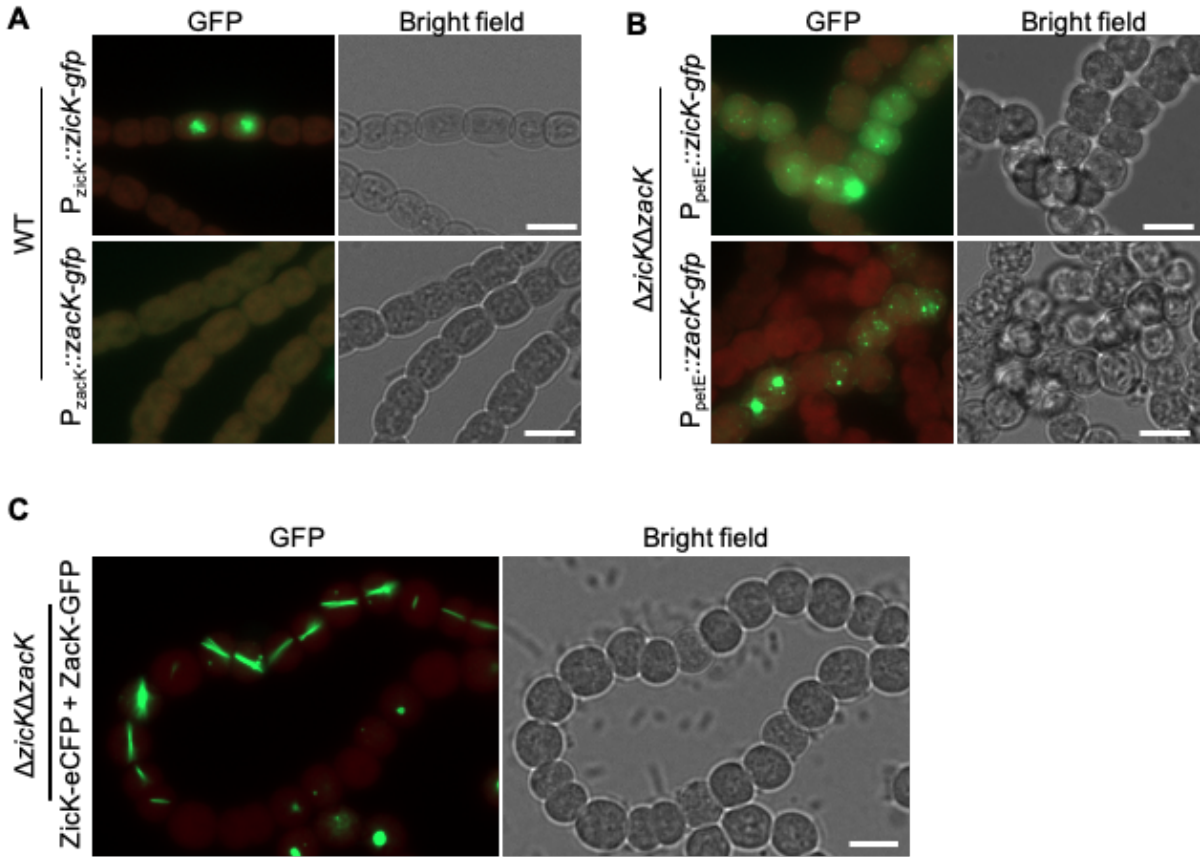

Supplementary Fig. 4: Heterologous expression of ZicK and ZacK

(**A**) Merged GFP fluorescence and chlorophyll autofluorescence (red) and bright field micrographs of *Anabaena* WT cells expressing ZicK-GFP or ZacK-GFP from P_{zicK} and P_{zacK}. No expression of ZacK-GFP is detectable from P_{zacK} while expression of ZicK-GFP from P_{zicK} leads to similar patchy clumps within the cells as observed from P_{petE} in Fig. 4A. Note, we generally observed that the P_{petE}-driven gene expression does not always lead to expression of the fusion protein in every cell under standard growth conditions. (**B,C**) Merged GFP fluorescence and chlorophyll autofluorescence and bright field micrographs of Δ*zicK*Δ*zacK* mutant expressing (**B**) ZicK-GFP or ZacK-GFP or (**C**) co-expressing ZicK-eCFP and ZacK-GFP from P_{petE}. For expression of ZicK-GFP alone, BG11 plates were supplemented with 1 µM $CuSO_4$. (**A-C**) These experiments show that expression of ZicK-GFP and ZacK-GFP or co-expression of ZicK-eCFP together with ZacK-GFP (Fig. 3A) from P_{petE} and their localization in *Anabaena* WT is not affected by ZicK or ZacK natively present in the WT background. Scale bars: (A-C) 5 µm.

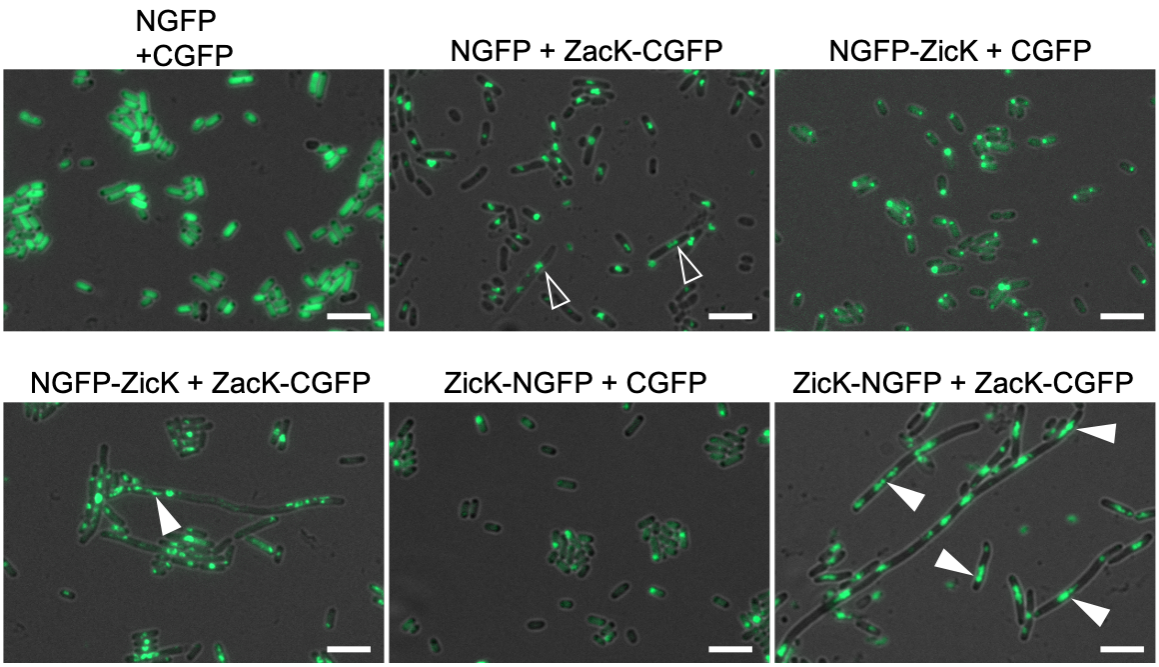

Supplementary Fig. 5: Host-independent heteropolymerization of ZicK and ZacK upon heterologous expression in *E. coli*

GFP-fragment reassembly assay. Merged GFP fluorescence and bright field micrographs of *E. coli* cells co-expressing NGFP (empty pET11a-link-NGFP) and CGFP (empty pMRBAD-link-CGFP), NGFP and ZacK-CGFP, NGFP-ZicK and CGFP, NGFP-ZicK and ZacK-CGFP, ZicK-NGFP and CGFP or ZicK-NGFP and ZacK-CGFP. Transparent triangles point to structures resembling ZacK-His *in vitro* polymers. White triangles indicate FilP-GFP-like (Bagchi *et al.*, 2008) filament-like structures that resemble structures indicated with translucent triangles but span longer distances. Co-expression of both, ZicK and ZacK leads to an elongated cell phenotype. FilP-like structures and elongated cells can already be seen upon co-expression of NGFP-ZicK with ZacK-CGFP but only the co-expression of ZicK and ZacK with C-terminal GFP-fragments leads to a clear filamentous cell phenotype and abundant intracellular filament-like structures. This suggests that the N-terminus of ZicK and ZacK is important for heteropolymerization. Note: we observed that the GFP-fragment reassembly assay is not suitable for the detection of protein-protein interaction strengths as even empty vector controls reconstitute the GFP protein, nonetheless, we employed it as a mean to localize the effect of co-expression of ZicK and ZacK in an entirely unrelated organism. Scale bars: 5 µm.

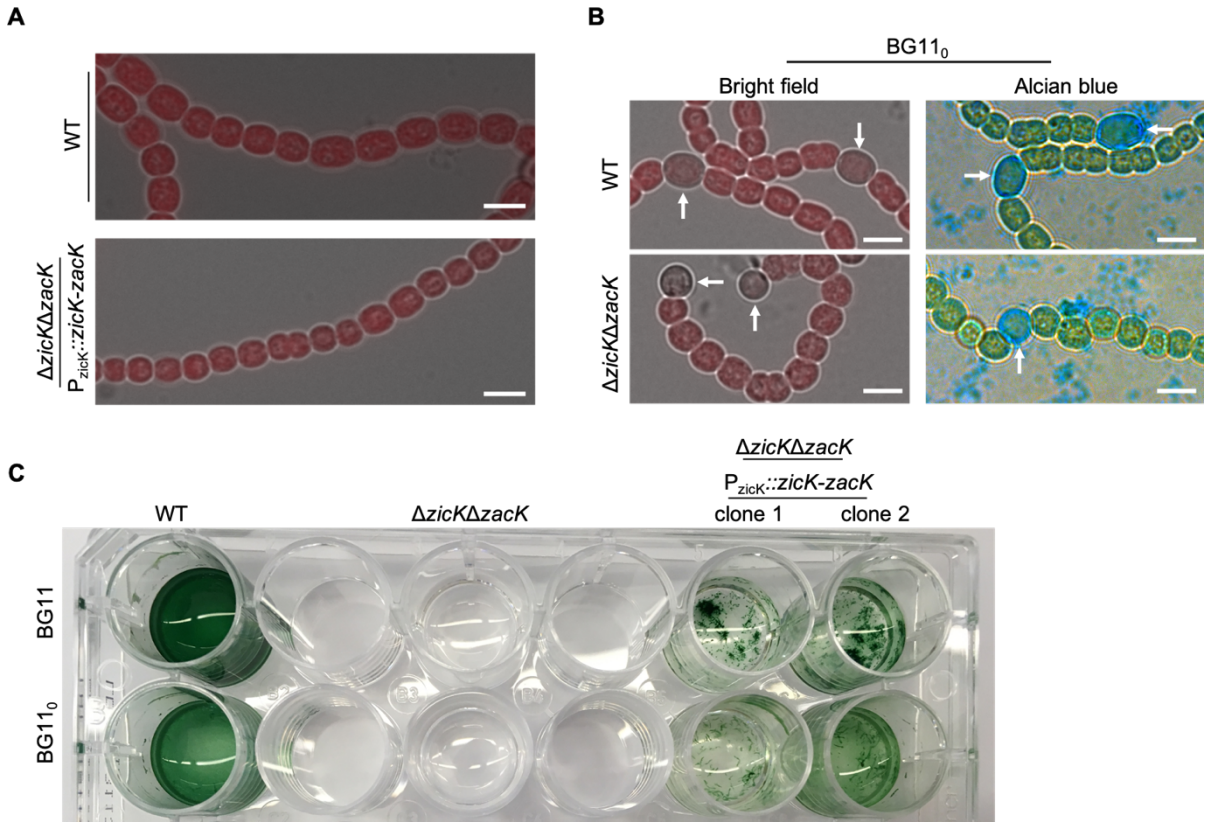

Supplementary Fig. 6: Mutant phenotype complementation and identification of heterocysts

(**A**) Morphological complementation of the ΔzicKΔ*zacK* mutant strain as a result of native expression of *zicK-zacK* from pRL25C. The capacity to complement the mutant phenotypes using the pRL25C plasmid shows that pDU1-based plasmids can be successfully employed to rescue WT phenotypes despite their variation in the relative copy number (Yang *et al.*, 2013). (**B**) Colour images of *Anabaena* WT and ΔzicKΔ*zacK* mutant strain grown on $BG11_0$ plates and stained with alcian blue. (**A**,**B**) Scale bars: 5 µm. (**C**) Rescue of liquid growth of the Δ*zicK*ΔzacK mutant strains by expressing *zicK-zacK* from P_{zicK} from the replicative pRL25C plasmid.

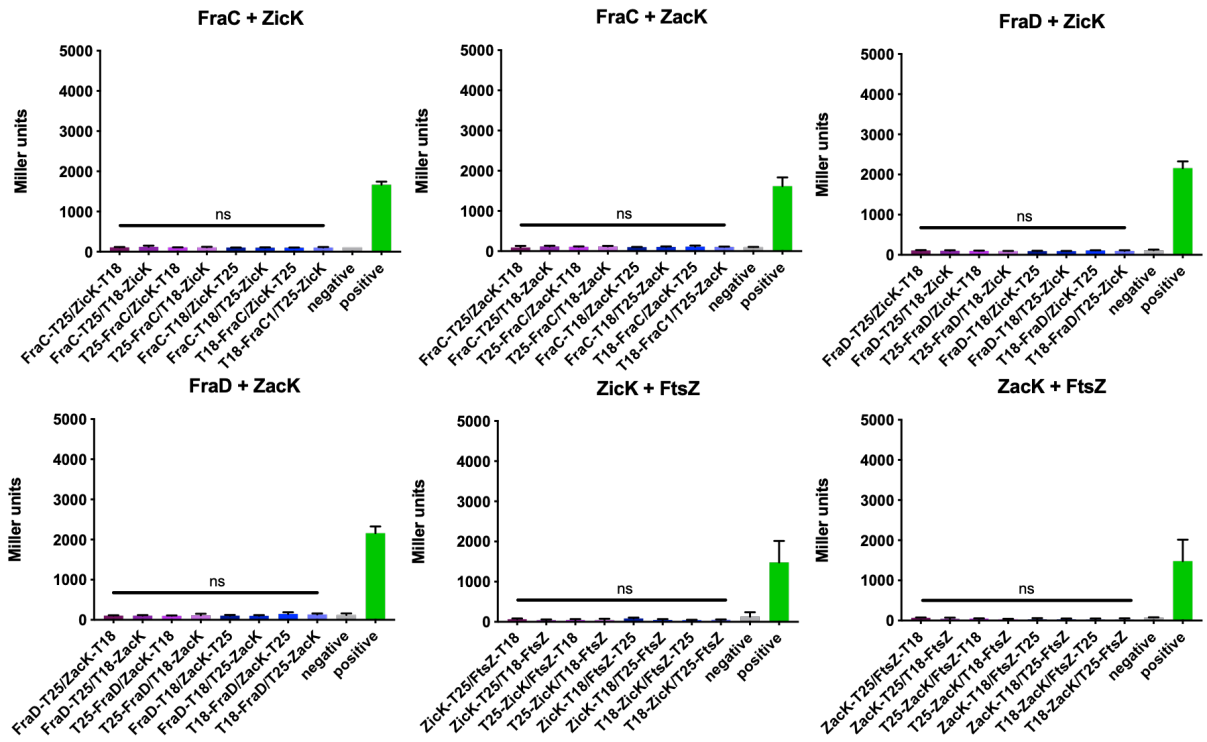

Supplementary Fig. 7: ZicK and ZacK do not interact with other components of the septal junctions besides SepJ

Beta-galactosidase assays of *E. coli* cells co-expressing indicated T25 and T18 translational fusions of all possible pair-wise combinations. Quantitative values are given in Miller units, and the mean results from three independent colonies are presented. Negative: N-terminal T25 fusion construct of the respective protein co-transformed with empty pUT18C. Positive: Zip/Zip control. Error bars indicate standard deviations (n = 3). *: P<0.05, **: P<0.01, ***: P<0.001, ****: P<0.0001 (Dunnett's multiple comparison test and one-way ANOVA).

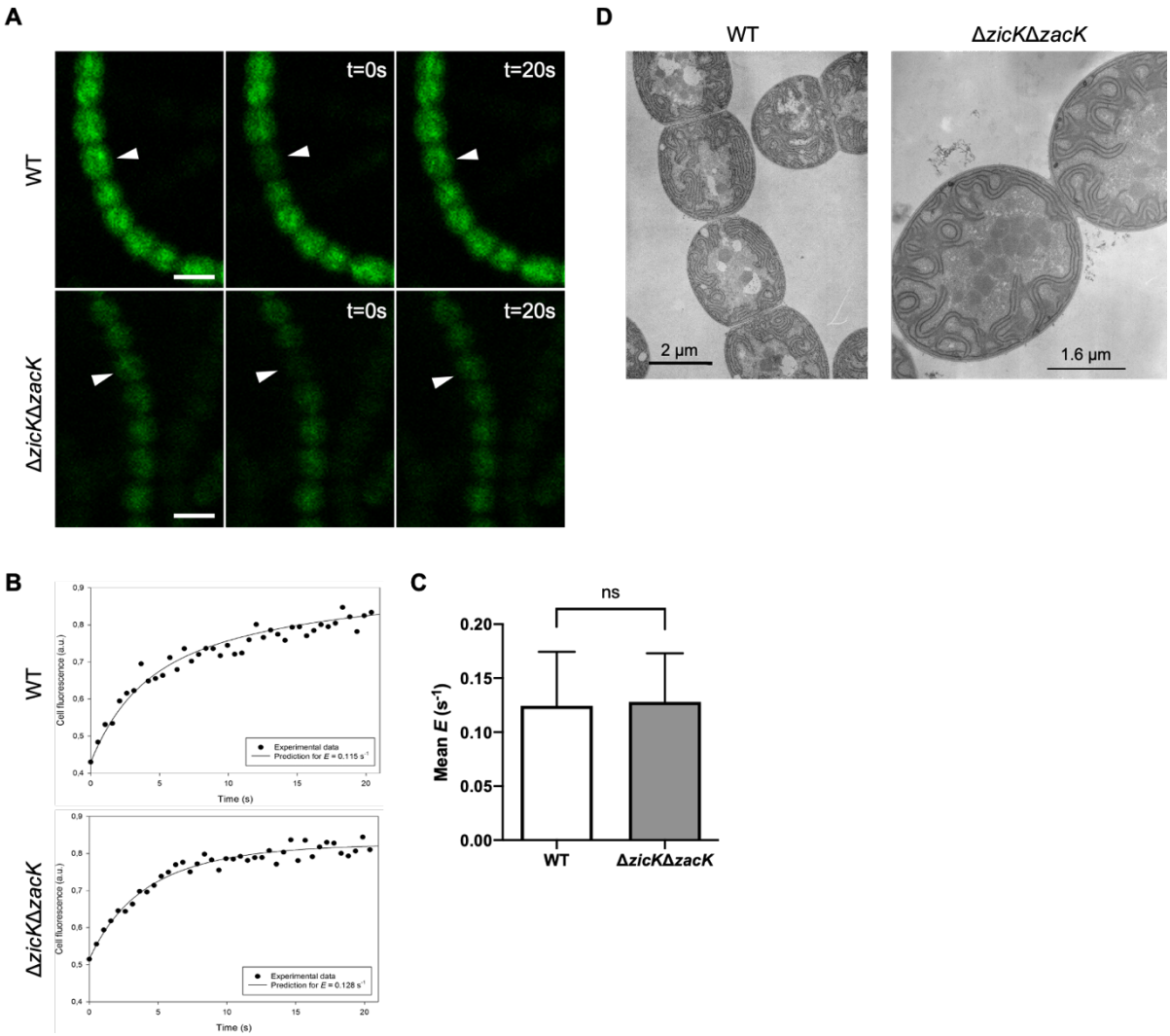

Supplementary Fig. 8: The Δ*zicK*Δ*zacK* mutant is not defective in intercellular transport and cellular ultrastructures

(**A**) Representative calcein fluorescence micrographs of FRAP experiments from calcein-labelled *Anabaena* WT and Δ*zicK*Δ*zacK* mutant grown on BG11 plates and (**B**) respective representative cell fluorescence recovery graphs. White triangles indicate bleached cells. Fluorescence images show respective cells prior bleaching, immediately after bleaching (t=0) and 20 seconds after bleaching (t=20s). Scale bars: 5 µm. **(C)** Mean exchange coefficients (E) of FRAP experiments from (**A**). Data present the number of recordings of bleached cells (*Anabaena* WT: n=21; Δ*zicK*Δ*zacK*: n=17). Values indicated with "ns" are not significantly different from the WT (using Student's t-test). (**D**) Ultrathin sections of *Anabaena* WT and Δ*zicK*Δ*zacK* mutant strain grown on BG11 plates.

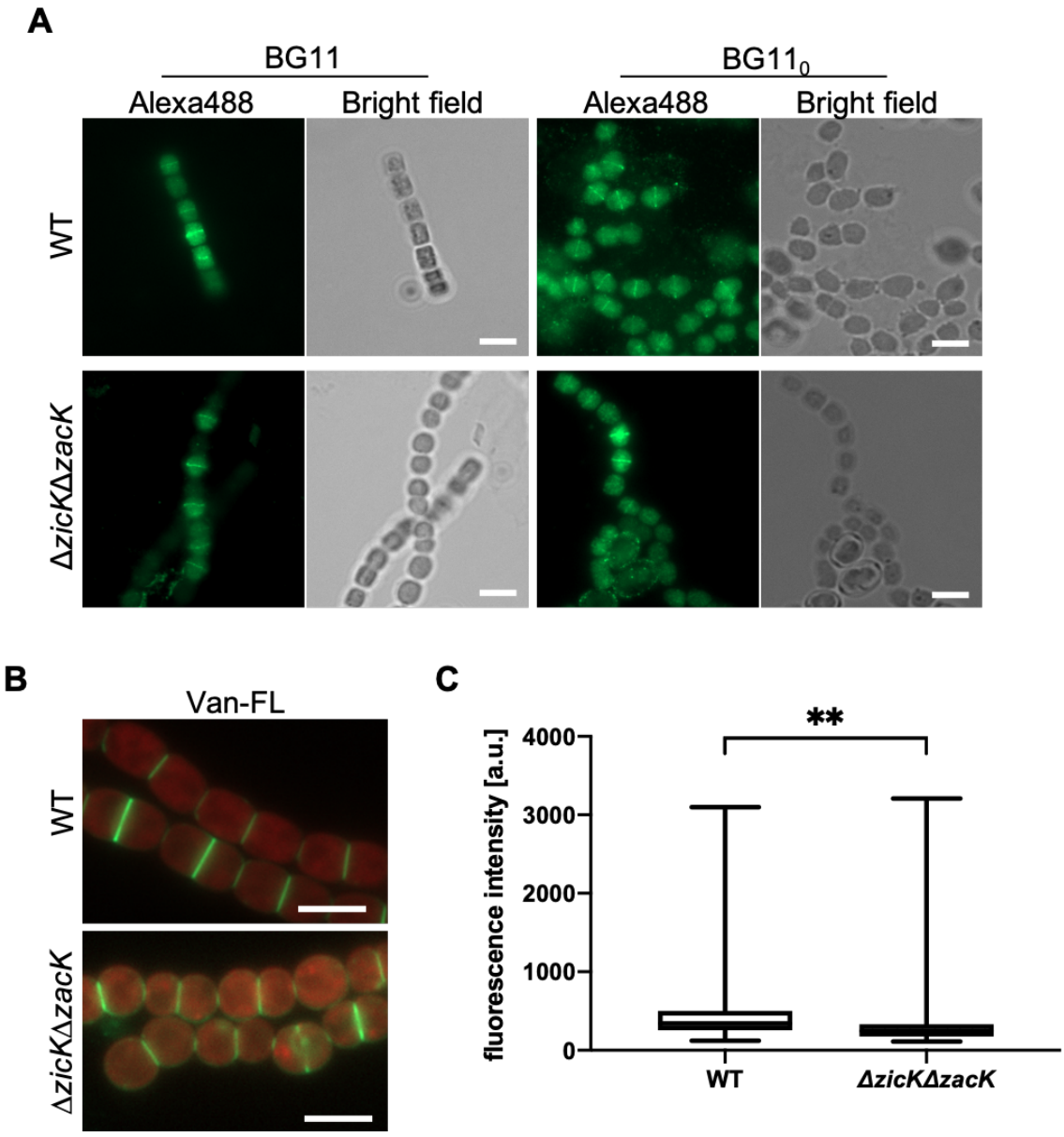

Supplementary Fig. 9: PG biogenesis and Z-ring placement are largely unaffected in the Δ*zicK*Δ*zacK* mutant

(**A**) Alexa Fluor-488 and bright field micrographs of Anabaena WT and Δ*zicK*Δ*zacK* mutant subjected to anti-FtsZ immunofluorescence. (**B**) Merged BODIPY™ FL Vancomycin (Van-FL) fluorescence and chlorophyll autofluorescence micrographs of *Anabaena* WT and the Δ*zicK*Δ*zacK* mutant stained with Van-FL. As a result of the low Van-FL staining and for better visibility, Van-FL fluorescence signal in Δ*zicK*Δ*zacK* mutant was artificially increased about twofold after image acquisition (note: this increase was not used for the fluorescence intensity measurement in (**C**)). Scale bars: (**A**,**B**) 5 µm. (**C**) Arithmetic mean fluorescence intensities of n=200 cell septa from (**B**). Values indicated with * are significantly different from the WT. **: P <.001, (Student's t-test).

Supplementary Table 1: Cyanobacterial strains

Strain	Genotype	Resistance marker	Source
Anabaena sp. PCC 7120	WT		Pasteur culture collection of Cyanobacteria (PCC)
BLS2	*Anabaena* (Δ*zicK*Δ*zacK*)::CS.3	Sp, Sm	This study

Sp = spectinomycin, Sm = streptomycin

Supplementary Table 2: *E. coli* strains

Strain	Genotype	Resistance	Source
DH5αMCR	F- *endA1 supE44 thi-1* λ^- *recA1 gyrA96 relA1 deoR* Δ(*lacZYA-argF*)U169 Φ80d*lacZ*ΔM15 *mcrA* Δ(*mrr* hsdRMS *mcrBC*)		(Grant *et al.*, 1990)
BL21 (DE3)	F^- *ompT gal dcm lon hsdS*$_B$($r_B^- m_B^-$) λ(DE3 [*lacI lacUV5-T7p07 ind1 sam7 nin5*]) [*malB*$^+$]$_{K\text{-}12}$(λ^S)		(Studier and Moffatt, 1986)
BTH101	F^-, *cya-99*, *araD139*, *galE15*, *galK16*, *rpsL1* (*Str*$_r$), *hsdR2, mcrA1*,*mcrB1*	Sm	Euromedex
XL1-blue	endA1 gyrA96(nal^R) thi-1 recA1 relA1 lac glnV44 F'[::Tn10 proAB$^+$ lacI^q Δ(*lacZ*)M15] *hsdR17*(r_K^- m_K^+)	Tet	Stratagene
HB101	F^- *mcrB mrr hsd*S20(r_B^- m_B^-) *rec*A13 *leuB*6 *ara*-14 *pro*A2 *lac*Y1 *gal*K2 *xyl*-5 mtl-1 rpsL20(Sm^R) glnV44 λ^-	Sm	(Boyer and Roulland-Dessoix, 1969)

Tet = tetracycline

Supplementary Table 3: Plasmids

Name	Description	Resistance	Source
pET21a(+)	Bacterial vector for expressing N- terminal T7 and/or C-terminal His6-tagged proteins in *E. coli*	Amp	Novagen
pIGA	Cyanobacterial vector for insertion into neutral locus (RS1 and RS2) of *slr0168* in *Synechocystis*	Amp, Km	A gift from Martin Hagemann (University Rostock, Germany); (Kunert *et al.*, 2000)
pRL25C	Shuttle cosmid vector for cyanobacteria and *E. coli*	Km, Nm	(Wolk *et al.*, 1988)
pRL623	Methylation plasmid	Cm	(Wolk *et al.*, 1988)
pRL443	Conjugation plasmid	Amp	(Wolk *et al.*, 1988)
pRL278	Suicide vector used for homologous recombination in cyanobacteria; contains *sacB* for positive selection of double recombination events	Km, Nm	(Wolk *et al.*, 1988)

pKNT25	P_{lac}::-*T25*	Km	Euromedex
pKT25	P_{lac}::*T25*-	Km	Euromedex
pUT18	P_{lac}::-*T18*	Amp	Euromedex
pUT18C	P_{lac}::*T18*-	Amp	Euromedex
pKT25-zip	pKT25; P_{lac}::*T25-zip*	Km, Nm	Euromedex
pUT18C-zip	pUT18C, P_{lac}::*T18-zip*	Amp	Euromedex
pET11a-link-NGFP	IPTG-inducible expression vector for translational fusion of target gene with a N-terminal *gfp* fragment in *E. coli*	Amp	(Wilson *et al.*, 2004)
pMRBAD-link-CGFP	L-arabinose-inducible expression vector for translational fusion of target gene with a C-terminal *gfp* fragment in *E. coli*	Km	(Wilson *et al.*, 2004)
pAM5084	P_{trc}::*ecfp-kaiC*	Amp	(Cohen *et al.*, 2014)
pCSEL24	Integrates into the *nucA-nuiA* region of *Anabaena*	Amp, Sm, Sp	(Olmedo-Verd *et al.*, 2006)
pTHS1	pRL25C, P_{petE}::*zicK-gfp*	Km, Nm	This study
pTHS4	pKNT25, P_{lac}::*zipM-T25*	Km, Nm	This study
pTHS5	pKT25, P_{lac}::*T25-zipM*	Km, Nm	This study
pTHS6	pUT18, P_{lac}::*zipM-T18*	Amp	This study
pTHS7	pUT18C, P_{lac}::*T18-zipM*	Amp	This study
pTHS8	pKNT25, P_{lac}::*sepJ-T25*	Km, Nm	This study
pTHS9	pKT25, P_{lac}::*T25-sepJ*	Km, Nm	This study
pTHS10	pUT18, P_{lac}::*sepJ-T18*	Amp	This study
pTHS11	pUT18C, P_{lac}::*T18-sepJ*	Amp	This study
pTHS12	pKNT25, P_{lac}::*ftsZ-T25*	Km, Nm	This study
pTHS13	pKT25, P_{lac}::*T25-ftsZ*	Km, Nm	This study
pTHS14	pUT18, P_{lac}::*ftsZ-T18*	Amp	This study
pTHS15	pUT18C, P_{lac}::*T18-ftsZ*	Amp	This study
pTHS16	pKNT25, P_{lac}::*mreB-T25*	Km, Nm	This study
pTHS17	pKT25, P_{lac}::*T25-mreB*	Km, Nm	This study
pTHS18	pUT18, P_{lac}::*mreB-T18*	Amp	This study
pTHS19	pUT18C, P_{lac}::*T18-mreB*	Amp	This study
pTHS20	pKNT25, P_{lac}::*fraC-T25*	Km, Nm	This study
pTHS21	pKT25, P_{lac}::*T25-fraC*	Km, Nm	This study
pTHS22	pUT18, P_{lac}::*fraC-T18*	Amp	This study
pTHS23	pUT18C, P_{lac}::*T18-fraC*	Amp	This study
pTHS24	pKNT25, P_{lac}::*fraD-T25*	Km, Nm	This study
pTHS25	pKT25, P_{lac}::*T25-fraD*	Km, Nm	This study
pTHS26	pUT18, P_{lac}::*fraD-T18*	Amp	This study
pTHS27	pUT18C, P_{lac}::*T18-fraD*	Amp	This study
pTHS28	pKNT25, P_{lac}::*hmpF*$_{Ana}$*-T25*	Km, Nm	This study
pTHS29	pKT25, P_{lac}::*T25-hmpF*$_{Ana}$	Km, Nm	This study
pTHS30	pUT18, P_{lac}::*hmpF*$_{Ana}$ *-T18*	Amp	This study
pTHS31	pUT18C, P_{lac}::*T18-hmpF*$_{Ana}$	Amp	This study

pTHS134	pKNT25, P_{lac}::*sepI-T25*	Km, Nm	(Springstein *et al.*, 2020a)
pTHS135	pKT25, P_{lac}::*T25-sepI*	Km, Nm	(Springstein *et al.*, 2020a)
pTHS136	pUT18, P_{lac}::*sepI-T18*	Amp	(Springstein *et al.*, 2020a)
pTHS137	pUT18C, P_{lac}::*T18-sepI*	Amp	(Springstein *et al.*, 2020a)
pTHS151	pRL25C, P_{petE}::*zacK-gfp*	Km, Nm	This study
pTHS152	pRL25C, P_{petE}::*zicK-ecfp*	Km, Nm	This study
pTHS153	pRL25C, P_{petE}::*zicK-ecfp*[b)], P_{petE}::*zacK-gfp*	Km, Nm	This study
pTHS154	pET21a(+), P_{T7}::*zicK-his*	Amp	This study
pTHS155	pET21a(+), P_{T7}::*zacK-his*	Amp	This study
pTHS156	pET11a-link-NGFP, P_{T7}::*ngfp-zicK*	Amp	This study
pTHS157	pET11a-link-NGFP, P_{T7}::*zicK-ngfp*	Amp	This study
pTHS158	pMRBAD-link-CGFP, P_{ara}::*zacK-cgfp*	Km	This study
pTHS159	pKNT25, P_{lac}::*zicK-T25*	Km, Nm	This study
pTHS159	pKT25, P_{lac}::*T25-zicK*	Km, Nm	This study
pTHS160	pUT18, P_{lac}::*zicK -T18*	Amp	This study
pTHS161	pUT18C, P_{lac}::*T18-zicK*	Amp	This study
pTHS162	pKNT25, P_{lac}::*zacK-T25*	Km, Nm	This study
pTHS163	pKT25, P_{lac}::*T25-zacK*	Km, Nm	This study
pTHS164	pUT18, P_{lac}::*zacK-T18*	Amp	This study
pTHS165	pUT18C, P_{lac}::*T18-zacK*	Amp	This study
pTHS166	pRL278, containing 1500 bp upstream of *zicK* and 1500 bp downstream of *zacK* flanking the CS.3 cassette	Nm, Km, Sm, Sp	This study
pTHS167	pRL25C, P_{zicK}::*zicK-gfp*	Nm, Km,	This study
pTHS168	pRL25C, P_{zacK}::*zacK-gfp*	Nm, Km,	This study
pTHS169	pRL25C, P_{zicK}::*zicK-zacK*	Nm, Km,	This study
pTHS170	pIGA, P_{cpc560}::*zicK-gfp*	Amp; Km	This study
pTHS171	pIGA, P_{cpc560}::*zacK-gfp*	Amp; Km	This study
pTHS172	pIGA, P_{cpc560}::*zicK-ecfp*; P_{cpc560}::*zacK-gfp*	Amp; Km	This study

Km = kanamycin, Nm = neomycin, Amp = ampicillin; Cm = chloramphenicol

- eCFP from (Cohen *et al.*, 2014) was adjusted for C-terminal translational fusion instead of N-terminal fusion. For this, a N-terminal Myc sequences followed by a seven amino acid linker (GSGSGSG) and an additional stop codon at the C-terminus were added.

Supplementary Table 4: Oligonucleotides

#	Given name	Sequence (5' - > 3')	Purpose
1	rnpB_intern_A	TGCTGGATAACGTCCAGTGC	RT-PCR for *rnpB*
2	rnpB_intern_B	GGTTTACCGAGCCAGTACCTC	RT-PCR for *rnpB*
3	Nos903_intern_A	TCAGCTAGACGTAAAGAGTGGC	RT-PCR for *zicK*
4	Nos903_intern_B	TAATTCTGCTGGGAATGCAGC	RT-PCR for *zicK*
5	Nos904_intern_A	TGGAATTAGCGAAGGGGTGG	RT-PCR for *zacK*
6	Nos904_intern_B	TGTTCATAGCCATCTGTTGCCA	RT-PCR for *zacK*
7	petE_903_Fwd	GAGATTATCAAAAAGGATCCCAGTACTCAGA ATTTTTTGCTGAGGTACT	Amplification of P_{petE} for pTHS1
8	petE_903_Rev	TTGAGTGCAACTGTCGTCATGGCGTTCTCCT AACCTGTAGTTTTATTTTT	Amplification of P_{petE} for pTHS1
9	pRL25-Nos903_Fwd	CTACAGGTTAGGAGAACGCCATGACGACAG TTGCACTCAAAGATAG	Amplification of *zicK* for pTHS1
10	pRL25-Nos903_Rev	GCACTAGCAGATGCACTAGCTTTAGCCGTA GAACTATCAAAAGCTCTCATTGC	Amplification of *zicK* for pTHS1
11	GFP_903_Fwd	TTGATAGTTCTACGGCTAAAGCTAGTGCATC TGCTAGTGCTAGT	Amplification of *gfp* for pTHS1
12	GFP_903_Rev	CTTTCGTCTTCAAGAATTCTTTATTTGTATAG TTCATCCATGCCATGTGTAATCC	Amplification of *gfp* for pTHS1
13	pRL25c-903_V_F	TGGATGAACTATACAAATAAAGAATTCTTGA AGACGAAAGGGCC	Amplification of pRL25C for pTHS1
14	pRL25c-903_V_R	GCAAAAAATTCTGAGTACTGGGATCCTTTTT GATAATCTCATGACCAAAATCC	Amplification of pRL25C for pTHS1
15	Nos904_2A	CTACAGGTTAGGAGAACGCCATGGCAGTCA AAAAGTTAACAGACAAAAAC	Amplification of zacK for pTHS151
16	Nos904_2B	GCACTAGCAGATGCACTAGCTTTATTTTTCA CTTGACTTTTTGCCTGTTCTAAAGC	Amplification of zacK for pTHS151
17	pRL25c_NEB_Fwd	GCTAGTGCATCTGCTAGTGCTAGTG	Amplification of pTHS1 to replace *zicK* with *zacK* (for pTHS151)
18	pRL25c_NEB_Rev	GGCGTTCTCCTAACCTGTAGTTTTATTTTTCT	Amplification of pTHS1 to replace *zicK* with *zacK* (for pTHS151
19	pRL25c_ClaI_B	ATAAGCTTTAATGCGGTAGTTTATCACAG	Amplification of pRL25C for pTHS152
20	pRL25c_ClaI_A	ATGATAAGCTGTCAAACATGAGAATTCTTG	Amplification of pRL25C for pTHS152
21	petE_2A	ACTACCGCATTAAAGCTTATCAGTACTCAGA ATTTTTTGCTGAGGTAC	Amplification of P_{petE}::*zicK* for pTHS152
22	Nos903_2B	ttcgctgataaGCTTCTGTTCTTTAGCCGTAGAAC TATCAAAAGCTCTC	Amplification of P_{petE}::*zicK* for pTHS152
23	Linker_eCFP_3A	GGCTCTGGATCGGGTTCAGGAATGGTGAGC AAGGGCGAG	First round of amplification of *ecfp* for pTHS152
24	eCFP_3B	CTGCTGCTTACTTGTACAGCTCGTCCATGCC	First round of amplification of *ecfp* for pTHS152 and pTHS172
25	MYC_Linker_3A2	GAACAGAAGCTTATCAGCGAAGAAGATCTG GGCTCTGGATCGGGTTCAG	Second round of amplification of

			ecfp for pTHS152 and pTHS172
26	eCFP_3B2	TCATGTTTGACAGCTTATCATTTACTTGTACA GCTCGTCCATGCC	Second round of amplification of *ecfp* for pTHS152
27	petE_BamHI_2A	TTGGTCATGAGATTATCAAAAAGCAGTACTC AGAATTTTTTGCTGAGG	Amplification of P_{petE}::*zacK-gfp* for pTHS153
28	GFP_BamHI_2B	ATTGATTTAAAACTTCATTTTTAATTTAAAAG TTATTTGTATAGTTCATCCATGCCATGTG	Amplification of P_{petE}::*zacK-gfp* for pTHS153
29	Nos903_NdeI_F	GCTACATATGACGACAGTTGCACTCA	Amplification of *zicK* for pTHS154
30	Nos903_XhoI_R_w/o	GCTACTCGAGTTTAGCCGTAGAACTATCAAA AGC	Amplification of *zicK* for pTHS154
31	Nos904_NdeI_F	GCTACATATGGCAGTCAAAAAGTTAACAGAC	Amplification of *zacK* for pTHS155
32	Nos904_XhoI_wo_R	GCTACTCGAGTTTATTTTTCACTTGACTTTTT GCCT	Amplification of *zacK* for pTHS155
33	903_split_A	AAGGTGGCTCTGGCTCTGGCTCGAGCATGA CGACAGTTGCACTCAAAG	Amplification of *zicK* for pTHS156
34	903_split_B	CGGGCTTTGTTAGCAGCCGTTATTTAGCCG TAGAACTATCAAAAGCTCTC	Amplification of *zicK* for pTHS156
35	903_split_A2	TTAACTTTAAGAAGGAGATATACATATGACG ACAGTTGCACTCAAAG	Amplification of *zicK* for pTHS157
36	903_split_B2	CCATGGTGATGGTGGTGATGAGATGCACTA GCTTTAGCCGTAGAACTATCAAAAGCTCT	Amplification of *zicK* for pTHS157
37	904_split_A	TTTAACTTTAAGAAGGAGATATACCATGGCA GTCAAAAAGTTAACAGACA	Amplification of *zacK* for pTHS158
38	904_split_B	TTACCGCTTCCACCCGACGTTTTATTTTTCA CTTGACTTTTTGCCTGTTC	Amplification of *zacK* for pTHS158
39	N-term_1A	GAGGATCCCCGGGTACC	PCR amplification of pKNT25 and pUT18
40	N-term_1B	TAGAGTCGACCTGCAGGCA	PCR amplification of pKNT25 and pUT18
41	pKT25_1A	CCCCGGGTACCTAAGTAAGTAAG	PCR amplification of pKT25
42	pKT25_1B	ATCCTCTAGAGTCGACCCTGC	PCR amplification of pKT25
43	pUT18C_1A	CCGAGCTCGAATTCATCGAT	PCR amplification of pUT18C
44	pUT18C_1B	TACCCGGGGATCCTCTAGAGT	PCR amplification of pUT18C
45	MB_17A	TGCCTGCAGGTCGACTCTAATGACGACAGT TGCACTCAAAG	Cloning of *zicK* into pKNT25 or pUT18
46	MB_17B	TCGGTACCCGGGGATCCTCTTTAGCCGTAG AACTATCAAAAGCTCTC	Cloning of *zicK* into pKNT25 or pUT18
47	MB_18A	AGGGTCGACTCTAGAGGATATGACGACAGT TGCACTCAAAG	Cloning of *zicK* into pKT25
48	MB_18B	CTTACTTAGGTACCCGGGGTTTAGCCGTAG AACTATCAAAAGCTCTC	Cloning of *zicK* into pKT25
49	MB_20A	TCTAGAGGATCCCCGGGTAATGACGACAGT TGCACTCAAAG	Cloning of *zicK* into pUT18C
50	MB_20B	TCGATGAATTCGAGCTCGGTTTAGCCGTAG AACTATCAAAAGCTCTC	Cloning of *zicK* into pUT18C

51	MB_21A	TGCCTGCAGGTCGACTCTAATGGCAGTCAA AAAGTTAACAGACAA	Cloning of *zacK* into pKNT25 or pUT18
52	MB_21B	TCGGTACCCGGGGATCCTCTTTATTTTTCAC TTGACTTTTTGCCTGTTC	Cloning of *zacK* into pKNT25 or pUT18
53	MB_22A	AGGGTCGACTCTAGAGGATATGGCAGTCAA AAAGTTAACAGACAA	Cloning of *zacK* into pKT25
54	MB_22B	CTTACTTAGGTACCCGGGGTTTATTTTTCAC TTGACTTTTTGCCTGTTC	Cloning of *zacK* into pKT25
55	MB_24A	TCTAGAGGATCCCCGGGTAATGGCAGTCAA AAAGTTAACAGACAA	Cloning of *zacK* into pUT18C
56	MB_24B	TCGATGAATTCGAGCTCGGTTTATTTTTCAC TTGACTTTTTGCCTGTTC	Cloning of *zacK* into pUT18C
57	MB_25A	TGCCTGCAGGTCGACTCTAATGCAACAAGT CATAGTAAGTAATCGAT	Cloning of *zipM* into pKNT25 or pUT18
58	MB_25B	TCGGTACCCGGGGATCCTCGGATGCGTATC TAGCTATTAGATGTTC	Cloning of *zipM* into pKNT25 or pUT18
59	MB_26A	AGGGTCGACTCTAGAGGATATGCAACAAGT CATAGTAAGTAATCGAT	Cloning of *zipM* into pKT25
60	MB_26B	CTTACTTAGGTACCCGGGGGGATGCGTATC TAGCTATTAGATGTTC	Cloning of *zipM* into pKT25
61	MB_28A	TCTAGAGGATCCCCGGGTAATGCAACAAGT CATAGTAAGTAATCGAT	Cloning of *zipM* into pUT18C
62	MB_28B	TCGATGAATTCGAGCTCGGGGATGCGTATC TAGCTATTAGATGTTC	Cloning of *zipM* into pUT18C
63	MB_41A	TGCCTGCAGGTCGACTCTAATGGGGCGATT TGAGAAGC	Cloning of *sepJ* into pKNT25 or pUT18
64	MB_41B	TCGGTACCCGGGGATCCTCACCTTCTGCAT TGGCAGG	Cloning of *sepJ* into pKNT25 or pUT18
65	MB_42A	AGGGTCGACTCTAGAGGATATGGGGCGATT TGAGAAGC	Cloning of *sepJ* into pKT25
66	MB_42B	CTTACTTAGGTACCCGGGGACCTTCTGCATT GGCAGG	Cloning of *sepJ* into pKT25
67	MB_44A	TCTAGAGGATCCCCGGGTAATGGGGCGATT TGAGAAGC	Cloning of *sepJ* into pUT18C
68	MB_44B	TCGATGAATTCGAGCTCGGACCTTCTGCATT GGCAGG	Cloning of *sepJ* into pUT18C
69	MB_49A	ATGCCTGCAGGTCGACTCTAATGACACTTG ATAATAACCAAGAGCTTACC	Cloning of *ftsZ* into pKNT25 or pUT18
70	MB_49B	CTCGGTACCCGGGGATCCTCATTTTTGGGT GGTCGCCGTC	Cloning of *ftsZ* into pKNT25 or pUT18
71	MB_50A	CAGGGTCGACTCTAGAGGATATGACACTTG ATAATAACCAAGAGCTTACC	Cloning of *ftsZ* into pKT25
72	MB_50B	TACTTACTTAGGTACCCGGGGATTTTTGGGT GGTCGCCGTC	Cloning of *ftsZ* into pKT25
73	MB_52A	CTCTAGAGGATCCCCGGGTAATGACACTTG ATAATAACCAAGAGCTTACC	Cloning of *ftsZ* into pUT18C
74	MB_52B	TATATCGATGAATTCGAGCTCGGATTTTTGG GTGGTCGCCGTC	Cloning of *ftsZ* into pUT18C
75	MB_53A	ATGCCTGCAGGTCGACTCTAATGGGGCTTT TTAGGAACTTTCG	Cloning of *mreB* into pKNT25 or pUT18
76	MB_53B	CTCGGTACCCGGGGATCCTCCATATTTCGA GATCGTCCGCTAAAAAC	Cloning of *mreB* into pKNT25 or pUT18

77	MB_54A	CAGGGTCGACTCTAGAGGATATGGGGCTTTTTAGGAACTTTCG	Cloning of *mreB* into pKT25
78	MB_54B	TACTTACTTAGGTACCCGGGGCATATTTCGAGATCGTCCGCTAAAAAC	Cloning of *mreB* into pKT25
79	MB_56A	CTCTAGAGGATCCCCGGGTAATGGGGCTTTTTAGGAACTTTCG	Cloning of *mreB* into pUT18C
80	MB_56B	TATATCGATGAATTCGAGCTCGGCATATTTCGAGATCGTCCGCTAAAAAC	Cloning of *mreB* into pUT18C
81	MB_69A	ATGCCTGCAGGTCGACTCTAATGTTTGAAGATTTGACTATACCCAGG	Cloning of *fraC* into pKNT25 or pUT18
82	MB_69B	CTCGGTACCCGGGGATCCTCCCTATTACGTATCAATAAAATAATAGTTATAGCGGTG	Cloning of *fraC* into pKNT25 or pUT18
83	MB_70A	CAGGGTCGACTCTAGAGGATATGTTTGAAGATTTGACTATACCCAGG	Cloning of *fraC* into pKT25
84	MB_70B	TACTTACTTAGGTACCCGGGGCCTATTACGTATCAATAAAATAATAGTTATAGCGGTG	Cloning of *fraC* into pKT25
85	MB_72A	CTCTAGAGGATCCCCGGGTAATGTTTGAAGATTTGACTATACCCAGG	Cloning of *fraC* into pUT18C
86	MB_72B	ATATCGATGAATTCGAGCTCGGCCTATTACGTATCAATAAAATAATAGTTATAGCGGTG	Cloning of *fraC* into pUT18C
87	MB_73A	ATGCCTGCAGGTCGACTCTAGTGAATTTATTATTTAAAGACCTTTTCGGAATATT	Cloning of *fraD* into pKNT25 or pUT18
88	MB_73B	CTCGGTACCCGGGGATCCTCCTGCTGCGGTGGCGCTG	Cloning of *fraD* into pKNT25 or pUT18
89	MB_74A	GGGTCGACTCTAGAGGATGTGAATTTATTATTTAAAGACCTTTTCGGAAT	Cloning of *fraD* into pKT25
90	MB_74B	TACTTACTTAGGTACCCGGGGCTGCTGCGGTGGCGCTG	Cloning of *fraD* into pKT25
91	MB_76A	CTAGAGGATCCCCGGGTAGTGAATTTATTATTTAAAGACCTTTTCGGAAT	Cloning of *fraD* into pUT18C
92	MB_76B	TATATCGATGAATTCGAGCTCGGCTGCTGCGGTGGCGCTG	Cloning of *fraD* into pUT18C
93	pRL271_Fwd	GAGCTCGCGAAAGCTTGCATG	Amplification of pRL278
94	pRL271_Rev	CTCGAGATCTAGATATCGAATTTCTGCCAT	Amplification of pRL278
95	CS.3_Fwd	GATCCGTGCACAGCACCTTG	Amplification of CS.3 cassette
96	CS.3_Rev	TTATTTGCCGACTACCTTGGTGATCT	Amplification of CS.3 cassette
97	903KO_2A	ATTCGATATCTAGATCTCGAGAAGCAACGGCAACGCC	Amplification of upstream homology region for *zicK+zacK* deletion
98	903KO_2B	AAGGTGCTGTGCACGGATCATTTCAACTCCCTTGATTAGATAATGATTAATCGAG	Amplification of upstream homology region for *zicK+zacK* deletion
99	904KO_4A	CAAGGTAGTCGGCAAATAAAATACAAATAATAAAAATAAATAAAAAGACGTAACGAAAATTACG	Amplification of downstream homology region for *zicK+zacK* deletion

100	904KO_4B	TGCAAGCTTTCGCGAGCTCGTAGTGGGTTTCGCACAAGCTATC	Amplification of downstream homology region for *zicK+zacK* deletion
101	903KO_Seq_A	TGCGAATTCCAGTAGGTCTTGGTAA	cPCR verification of *zicK and zacK deletion*
102	904KO_Seq_B	GGTGGCGCAGAAGTATTTTTG	cPCR verification of *zicK and zacK deletion*
103	p903_25C_long_A	TTTTGGTCATGAGATTATCAAAAAGACCCGACACTCTTGAGG	Amplification of P_{zicK}::*zicK-zacK* for pTHS169 and amplification of P_{zicK} for pTHS167
104	Nos904_25C_B	GGCCCTTTCGTCTTCAAGTTATTTATTTTTCACTTGACTTTTTGCCTGT	Amplification of P_{zicK}::*zicK-zacK* for pTHS169
105	pNos903_2B	ACTGTCGTCATATTTCAACTCCCTTG	Amplification of P_{zicK} for pTHS167
106	Nos903_pNos903_3A	GGAGTTGAAATATGACGACAGTTGCACTCAAAG	Amplification of *zicK-gfp* for pTHS167
107	GFP_25C_R	AGGCCCTTTCGTCTTCAAGTTATTTGTATAGTTCATCCATGCCATGTGT	Amplification of *zicK-gfp* or *zacK-gfp* for pTHS167 or pTHS168
108	pNos904_25C_F	ATTTTGGTCATGAGATTATCAAAAAGAGAAATATCAGCTAGACGTAAAGAGTGG	Amplification of P_{zacK} for pTHS168
109	pNos904_2B	TGACTGCCATAAAAACCTCTATTTATTGC	Amplification of P_{zacK} for pTHS168
110	Nos904_pNos904_3A	AGAGGTTTTTATGGCAGTCAAAAAGTTAACAGACAAAAAC	Amplification of *zacK-gfp* for pTHS168
111	Vector.FOR	TGATGTTCAACTTCGACAGCGAATTCCTCGACCTGCAGGG	Amplification of pIGA
112	Vector.REV	AGGGACTCTTCTCTACAGGTGGTACCCCGGGTTCGAAATCG	Amplification of pIGA
113	Fragment 1.FOR	GATTTCGAACCCGGGGTACCACCTGTAGAGAAGAGTCCCTGAATATCAA	Amplification of P_{cpc560} for pTHS170 and pTHS171
114	pIGA_Pcpc560_1B	TGAATTAATCTCCTACTTGACTTTATGAGTTGGG	Amplification of P_{cpc560} for pTHS170 and pTHS171
115	Nos903_pIGA_2A	TAAAGTCAAGTAGGAGATTAATTCAATGACGACAGTTGCACTCAAAG	Amplification of *zicK-gfp* for pTHS170
116	Fragment 3.REV	CCGACAATCCAAACACCGGTTTATTTGTATAGTTCATCCATGCCATGTGTAATCC	Amplification of *gfp* for pTHS170 and pTHS171
117	Fragment 4.FOR	TGGATGAACTATACAAATAAACCGGTGTTTGGATTGTCGG	Amplification of T_{rbcL} for pTHS170 and pTHS171
118	Fragment 4.REV	CCCTGCAGGTCGAGGAATTCGCTGTCGAAGTTGAACATCAGTAAGC	Amplification of T_{rbcL} for pTHS170 and pTHS171

119	Nos904_pIGA_2A	TAAAGTCAAGTAGGAGATTAATTCAATGGCA GTCAAAAAGTTAACAGACA	Amplification of *zacK-gfp* for pTHS171
120	Pcpc560_pIGA_A	AGGAGGAACTATATCCGGATACCTGTAGAG AAGAGTCCCTGAATATC	Amplification of P_{cpc560}::*zicK* for pTHS172
121	CFP_pIGA_B	ACCACACCCGTCCTGTGGATTTACTTGTACA GCTCGTCCATGCC	Second round of amplification of *ecfp* for pTHS172

Employed enzymatic cut sites are underlined.

References

Alberts, B., Johnson, A., Lewis, J., Morgan, D., Raff, M., Roberts, K., and Walter, P. (2014) *Molecular Biology of the Cell*. 6th editio., Garland Science, .

Altschul, S.F., Gish, W., Miller, W., Myers, E.W., and Lipman, D.J. (1990) Basic local alignment search tool. *J Mol Biol* **215**: 403–410 https://www.sciencedirect.com/science/article/pii/S0022283605803602?via%3Dihub. Accessed January 26, 2019.

Ausmees, N., Kuhn, J.R., and Jacobs-Wagner, C. (2003) The bacterial cytoskeleton: An intermediate filament-like function in cell shape. *Cell* **115**: 705–713.

Bagchi, S., Tomenius, H., Belova, L.M., and Ausmees, N. (2008) Intermediate filament-like proteins in bacteria and a cytoskeletal function in Streptomyces. *Mol Microbiol* **70**: 1037–1050.

Bermudes, D., Hinkle, G., and Margulis, L. (1994) Do prokaryotes contain microtubules? *Microbiol Rev* **58**: 387–400.

Bhaya, D., Takahashi, A., Shahi, P., and Arthur, R. (2001) Novel Motility Mutants of Synechocystis Strain PCC 6803 Generated by In Vitro Transposon Mutagenesis Novel Motility Mutants of Synechocystis Strain PCC 6803 Generated by In Vitro Transposon Mutagenesis †. *J Bacteriol* **183**: 1–5.

Bi, E., and Lutkenhaus, J. (1991) FtsZ ring structure associated with division in Escherichia coli. *Nature* **354**: 161–164 http://www.nature.com/doifinder/10.1038/354161a0.

Birchler, J.A., Bhadra, U., Bhadra, M.P., and Auger, D.L. (2001) Dosage-Dependent Gene Regulation in Multicellular Eukaryotes: Implications for Dosage Compensation, Aneuploid Syndromes, and Quantitative Traits. *Dev Biol* **234**: 275–288 http://www.sciencedirect.com/science/article/pii/S0012160601902623.

Blaauwen, T. den, Hamoen, L.W., and Levin, P.A. (2017) The divisome at 25: the road ahead. *Curr Opin Microbiol* **36**: 85–94 http://dx.doi.org/10.1016/j.mib.2017.01.007.

Boer, P. de, Crossley, R., and Rothfield, L. (1992) The essential bacterial cell-division protein FtsZ is a GTPase. *Nature* **359**: 254–256 http://www.nature.com/doifinder/10.1038/359254a0.

Boratyn, G.M., Schäffer, A.A., Agarwala, R., Altschul, S.F., Lipman, D.J., and Madden, T.L. (2012) Domain enhanced lookup time accelerated BLAST. *Biol Direct* **7**: 12 https://pubmed.ncbi.nlm.nih.gov/22510480.

Bornikoel, J., Carrión, A., Fan, Q., Flores, E., Forchhammer, K., Mariscal, V., *et al.* (2017) Role of Two Cell Wall Amidases in Septal Junction and Nanopore Formation in the Multicellular Cyanobacterium Anabaena sp. PCC 7120. *Front Cell Infect Microbiol* **7**: 386.

Boyer, H., and Roulland-Dessoix, D. (1969) A complementation analysis of the restrcition and modification of DNA in Escherichia coli. *J Mol Biol* **41**: 459–472.

Burnat, M., Schleiff, E., and Flores, E. (2014) Cell envelope components influencing filament length in the heterocyst-forming cyanobacterium Anabaena sp. strain PCC 7120. *J Bacteriol* **196**: 4026–4035.

Cabeen, M.T., Charbon, G., Vollmer, W., Born, P., Ausmees, N., Weibel, D.B., and Jacobs-Wagner, C. (2009) Bacterial cell curvature through mechanical control of cell growth. *EMBO J* **28**: 1208–1219 http://emboj.embopress.org/cgi/doi/10.1038/emboj.2009.61.

Cabeen, M.T., Herrmann, H., and Jacobs-Wagner, C. (2011) The domain organization of the bacterial intermediate filament-like protein crescentin is important for assembly and function.

Cytoskeleton **68**: 205–219.

Cai, Y., and Wolk, C.P. (1990) Use of a conditionally lethal gene in Anabaena sp. strain PCC 7120 to select for double recombinats and to entrap insertion sequnces. *J Bacteriol* **172**: 3138–3145.

Camargo, S., Picossi, S., Corrales-Guerrero, L., Valladares, A., Arévalo, S., and Herrero, A. (2019) ZipN is an essential FtsZ membrane tether and contributes to the septal localization of SepJ in the filamentous cyanobacterium Anabaena. *Sci Rep* **9**: 1–15.

Camberg, J.L., Hoskins, J.R., and Wickner, S. (2009) ClpXP protease degrades the cytoskeletal protein, FtsZ, and modulates FtsZ polymer dynamics. *Proc Natl Acad Sci U S A* **106**: 10614–10619 http://www.ncbi.nlm.nih.gov/pubmed/19541655.

Charbon, G., Cabeen, M.T., and Jacobs-Wagner, C. (2009) Bacterial intermediate filaments: In vivo assembly, organization, and dynamics of crescentin. *Genes Dev* **23**: 1131–1144.

Chen, C., MacCready, J.S., Ducat, D.C., and Osteryoung, K.W. (2018) The molecular machinery of chloroplast division. *Plant Physiol* **176**: 138–151.

Cho, Y.W., Gonzales, A., Harwood, T. V, Huynh, J., Hwang, Y., Park, J.S., *et al.* (2017) Dynamic localization of HmpF regulates type IV pilus activity and directional motility in the filamentous cyanobacterium Nostoc punctiforme. *Mol Microbiol* **106**: 252–265.

Choi, Y., Kim, J., Yoon, H.-J., Jin, K.S., Ryu, S., and Lee, H.H. (2018) Structural Insights into the FtsQ/FtsB/FtsL Complex, a Key Component of the Divisome. *Sci Rep* **8**: 18061 https://pubmed.ncbi.nlm.nih.gov/30584256.

Claessen, D., Rozen, D.E., Kuipers, O.P., Søgaard-Andersen, L., and Wezel, G.P. Van (2014) Bacterial solutions to multicellularity: A tale of biofilms, filaments and fruiting bodies. *Nat Rev Microbiol* **12**: 115–124 http://dx.doi.org/10.1038/nrmicro3178.

Cohen, S.E., Erb, M.L., Selimkhanov, J., Dong, G., Hasty, J., Pogliano, J., and Golden, S.S. (2014) Dynamic localization of the cyanobacterial circadian clock proteins. *Curr Biol* **24**: 1836–1844 http://dx.doi.org/10.1016/j.cub.2014.07.036.

Corrales-Guerrero, L., Camargo, S., Valladares, A., Picossi, S., Luque, I., Ochoa De Alda, J.A.G., and Herrero, A. (2018) FtsZ of filamentous, heterocyst-forming cyanobacteria has a conserved N-terminal peptide required for normal FtsZ polymerization and cell division. *Front Microbiol* **9**: 1–20.

Corrales-Guerrero, L., Mariscal, V., Flores, E., and Herrero, A. (2013) Functional dissection and evidence for intercellular transfer of the heterocyst-differentiation PatS morphogen. *Mol Microbiol* **88**: 1093–1105.

Dagan, T., Roettger, M., Stucken, K., Landan, G., Koch, R., Major, P., *et al.* (2013) Genomes of stigonematalean cyanobacteria (subsection V) and the evolution of oxygenic photosynthesis from prokaryotes to plastids. *Genome Biol Evol* **5**: 31–44.

Daniel, R.A., and Errington, J. (2003) Control of cell morphogenesis in bacteria: Two distinct ways to make a rod-shaped cell. *Cell* **113**: 767–776.

Du, Y., Cai, Y., Hou, S., and Xu, X. (2012) Identification of the HetR Recognition Sequence Upstream of hetZ in Anabaena sp. Strain PCC 7120. *J Bacteriol* **194**: 2297 LP – 2306 http://jb.asm.org/content/194/9/2297.abstract.

Ehira, S., Ohmori, M., and Sato, N. (2005) Identification of Low-temperature-regulated ORFs in the Cyanobacterium Anabaena sp. Strain PCC 7120: Distinguishing the Effects of Low

Temperature from the Effects of Photosystem II Excitation Pressure. *Plant Cell Physiol* **46**: 1237–1245 https://doi.org/10.1093/pcp/pci132.

England, P., Bourhy, P., Picardeau, M., Girons, I. Saint, Mazouni, K., and Pehau-Arnaudet, G. (2005) The Scc Spirochetal Coiled-Coil Protein Forms Helix-Like Filaments and Binds to Nucleic Acids Generating Nucleoprotein Structures. *J Bacteriol* **188**: 469–476.

Ent, F. van den, Amos, L.A., and Löwe, J. (2001) Prokrayotic origin of the actin cytoskeleton. *Nature* **413**: 39–44 vanDenEnt_2001_Nature_413(9)-39.pdf.

Erickson, H.P. (2007) Evolution of the cytoskeleton. *Bioessays* **29**: 668–677.

Errington, J., and Wu, L.J. (2017) Cell Cycle Machinery in Bacillus subtilis. Springer, Cham, pp. 67–101 http://link.springer.com/10.1007/978-3-319-53047-5_3. Accessed February 18, 2018.

Fenton, A.K., Mortaji, L. El, Lau, D.T.C., Rudner, D.Z., and Bernhardt, T.G. (2016) CozE is a member of the MreCD complex that directs cell elongation in Streptococcus pneumoniae. *Nat Microbiol* **2**: 1–9 http://dx.doi.org/10.1038/nmicrobiol.2016.237.

Fiedler, G., Arnold, M., Hannus, S., and Maldener, I. (1998) The DevBCA exporter is essential for envelope formation in heterocysts of the cyanobacterium Anabaena sp. strain PCC 7120. *Mol Microbiol* **27**: 1193–1202 https://doi.org/10.1046/j.1365-2958.1998.00762.x.

Flärdh, K., Richards, D.M., Hempel, A.M., Howard, M., and Buttner, M.J. (2012) Regulation of apical growth and hyphal branching in Streptomyces. *Curr Opin Microbiol* **15**: 737–743 http://www.sciencedirect.com/science/article/pii/S136952741200152X.

Flores, E., Herrero, A., Forchhammer, K., and Maldener, I. (2016) Septal Junctions in Filamentous Heterocyst-Forming Cyanobacteria. *Trends Microbiol* **24**: 79–82 http://dx.doi.org/10.1016/j.tim.2015.11.011.

Flores, E., Nieves-Morión, M., and Mullineaux, C. (2018) Cyanobacterial Septal Junctions: Properties and Regulation. *Life* **9**: 1.

Flores, E., Pernil, R., Muro-Pastor, A.M., Mariscal, V., Maldener, I., Lechno-Yossef, S., *et al.* (2007) Septum-localized protein required for filament integrity and diazotrophy in the heterocyst-forming cyanobacterium Anabaena sp. strain PCC 7120. *J Bacteriol* **189**: 3884–3890.

Fröjd, M.J., and Flärdh, K. (2019) Apical assemblies of intermediate filament-like protein FilP are highly dynamic and affect polar growth determinant DivIVA in Streptomyces venezuelae. *Mol Microbiol* **112**: 47–61.

Fuchs, E., and Weber, K. (1994) INTERMEDIATE FILAMENTS: Structure, Dynamics, Function and Disease. *Annu Rev Biochem* **63**: 345–382.

Grant, S.G., Jessee, J., Bloom, F.R., and Hanahan, D. (1990) Differential plasmid rescue from transgenic mouse DNAs into Escherichia coli methylation-restriction mutants. *Proc Natl Acad Sci* **87**: 4645–4649 http://www.pnas.org/cgi/doi/10.1073/pnas.87.12.4645.

Heins, S., and Aebi, U. (1994) Making heads and tails of intermediate filament assembly, dynamics and networks. *Curr Opin Cell Biol* **6**: 25–33.

Herrero, A., Stavans, J., and Flores, E. (2016) The multicellular nature of filamentous heterocyst-forming cyanobacteria. *FEMS Microbiol Rev* **40**: 831–854.

Herrmann, H., and Aebi, U. (2000) Intermediate filaments and their associates: Multi-talented structural elements specifying cytoarchitecture and cytodynamics. *Curr Opin Cell Biol* **12**: 79–

90.

Holmes, N.A., Walshaw, J., Leggett, R.M., Thibessard, A., Dalton, K.A., Gillespie, M.D., *et al.* (2013) Coiled-coil protein Scy is a key component of a multiprotein assembly controlling polarized growth in Streptomyces. *Proc Natl Acad Sci* **110**: E397–E406 http://www.pnas.org/cgi/doi/10.1073/pnas.1210657110.

Hu, B., Yang, G., Zhao, W., Zhang, Y., and Zhao, J. (2007) MreB is important for cell shape but not for chromosome segregation of the filamentous cyanobacterium Anabaena sp. PCC 7120. *Mol Microbiol* **63**: 1640–1652.

Ingerson-Mahar, M., Briegel, A., Werner, J.N., Jensen, G.J., and Gitai, Z. (2010) The metabolic enzyme CTP synthase forms cytoskeletal filaments. *Nat Cell Biol* **12**: 739–746.

Javadi, A., Söderholm, N., Olofsson, A., Flärdh, K., and Sandblad, L. (2019) Assembly mechanisms of the bacterial cytoskeletal protein FilP. *Life Sci Alliance* **2**: e201800290.

Jensen, T.E., and Ayala, R.P. (1980) Microtubule-like Inclusions in Isolates of the Blue-green Bacteria Anabaena and Nostoc. *Cytologia (Tokyo)* **45**: 315–326.

Jones, L.J.F., Carballido-López, R., and Errington, J. (2001) Control of cell shape in bacteria: Helical, actin-like filaments in Bacillus subtilis. *Cell* **104**: 913–922.

Karimova, G., Davi, M., and Ladant, D. (2012) The β-lactam resistance protein Blr, a small membrane polypeptide, is a component of the Escherichia coli cell division machinery. *J Bacteriol* **194**: 5576–5588.

Kelemen, G.H. (2017) Intermediate Filaments Supporting Cell Shape and Growth in Bacteria BT - Prokaryotic Cytoskeletons: Filamentous Protein Polymers Active in the Cytoplasm of Bacterial and Archaeal Cells. In Löwe, J., and Amos, L.A. (eds). Springer International Publishing, Cham. pp. 161–211 https://doi.org/10.1007/978-3-319-53047-5_6.

Kieninger, A.K., Forchhammer, K., and Maldener, I. (2019) A nanopore array in the septal peptidoglycan hosts gated septal junctions for cell-cell communication in multicellular cyanobacteria. *Int J Med Microbiol* **309**: 151303 https://doi.org/10.1016/j.ijmm.2019.03.007.

Klint, J., Rasmussen, U., and Bergman, B. (2007) FtsZ may have dual roles in the filamentous cyanobacterium Nostoc/Anabaena sp. strain PCC 7120. *J Plant Physiol* **164**: 11–18.

Köster, S., Weitz, D.A., Goldman, R.D., Aebi, U., and Herrmann, H. (2015) Intermediate filament mechanics in vitro and in the cell: From coiled coils to filaments, fibers and networks. *Curr Opin Cell Biol* **32**: 82–91.

Kühn, J., Briegel, A., Mörschel, E., Kahnt, J., Leser, K., Wick, S., *et al.* (2010) Bactofilins, a ubiquitous class of cytoskeletal proteins mediating polar localization of a cell wall synthase in Caulobacter crescentus. *EMBO J* **29**: 327–339.

Kunert, A., Hagemann, M., and Erdmann, N. (2000) Construction of promoter probe vectors for Synechocystis sp. PCC 6803 using the light-emitting reporter systems Gfp and LuxAB. *J Microbiol Methods* **41**: 185–194.

Lázaro, S., Fernández-Piñas, F., Fernández-Valiente, E., Blanco-Rivero, A., and Leganés, F. (2001) pbpB, a gene coding for a putative penicillin-binding protein, is required for aerobic nitrogen fixation in the cyanobacterium Anabaena sp. strain PCC7120. *J Bacteriol* **183**: 628–636.

Leganés, F., Blanco-Rivero, A., Fernández-Piñas, F., Redondo, M., Fernández-Valiente, E., Fan, Q., *et al.* (2005) Wide variation in the cyanobacterial complement of presumptive penicillin-binding proteins. *Arch Microbiol* **184**: 234–248.

Lehner, J., Berendt, S., Dörsam, B., Pérez, R., Forchhammer, K., and Maldener, I. (2013) Prokaryotic multicellularity: A nanopore array for bacterial cell communication. *FASEB J* **27**: 2293–2300.

Letek, M., Ordóñez, E., Vaquera, J., Margolin, W., Flärdh, K., Mateos, L.M., and Gil, J.A. (2008) DivIVA is required for polar growth in the MreB-lacking rod-shaped actinomycete Corynebacterium glutamicum. *J Bacteriol* **190**: 3283–3292.

Leung, C.L., Green, K.J., and Liem, R.K.H. (2002) Plakins: A family of versatile cytolinker proteins. *Trends Cell Biol* **12**: 37–45.

Lin, L., and Thanbichler, M. (2013) Nucleotide-independent cytoskeletal scaffolds in bacteria. *Cytoskeleton* **70**: 409–423.

Löwe, J., and Amos, L.A. (1998) Crystal structure of the bacterial cell division protein FtsZ. *Nature* **391**: 203–206.

Lupas, A., Dyke, M. Van, and Stock, J. (1991) Predicting coiled coils from protein sequences. *Science (80-)* **252**: 1162–1164 http://www.sciencemag.org/cgi/doi/10.1126/science.252.5009.1162.

Lutkenhaus, J. (2012) The ParA/MinD family puts things in their place. *Trends Microbiol* **20**: 411–418.

MacCready, J.S., Schossau, J., Osteryoung, K.W., and Ducat, D.C. (2017) Robust Min-system oscillation in the presence of internal photosynthetic membranes in cyanobacteria. *Mol Microbiol* **103**: 483–503.

Marchler-Bauer, A., Bo, Y., Han, L., He, J., Lanczycki, C.J., Lu, S., *et al.* (2016) CDD/SPARCLE: functional classification of proteins via subfamily domain architectures. *Nucleic Acids Res* **45**: D200–D203.

Mason, J.M., and Arndt, K.M. (2004) Coiled coil domains: Stability, specificity, and biological implications. *ChemBioChem* **5**: 170–176.

Mohr, R., Voß, B., Schliep, M., Kurz, T., Maldener, I., Adams, D.G., *et al.* (2010) A new chlorophyll d-containing cyanobacterium: evidence for niche adaptation in the genus Acaryochloris. *ISME J* **4**: 1456–1469 https://doi.org/10.1038/ismej.2010.67.

Mullineaux, C.W., Mariscal, V., Nenninger, A., Khanum, H., Herrero, A., Flores, E., and Adams, D.G. (2008) Mechanism of intercellular molecular exchange in heterocyst-forming cyanobacteria. *EMBO J* **27**: 1299–1308.

Nieves-Morión, M., Lechno-Yossef, S., López-Igual, R., Frías, J.E., Mariscal, V., Nürnberg, D.J., *et al.* (2017) Specific Glucoside Transporters Influence Septal Structure and Function in the Filamentous, Heterocyst-Forming Cyanobacterium Anabaena sp. Strain PCC 7120. *J Bacteriol* **199**: e00876-16 https://www.ncbi.nlm.nih.gov/pubmed/28096449.

Nogales, E., Downing, K.H., Amos, L.A., and Löwe, J. (1998) Tubulin and FtsZ form a distinct family of GTPases. *Nat Struct Biol* **5**: 451–458.

Olmedo-Verd, E., Muro-Pastor, A.M., Flores, E., and Herrero, A. (2006) Localized induction of the ntcA regulatory gene in developing heterocysts of Anabaena sp. strain PCC 7120. *J Bacteriol* **188**: 6694–6699.

Park, A., Jeong, H.-H., Lee, J., Kim, K.P., and Lee, C.-S. (2011) Effect of shear stress on the formation of bacterial biofilm in a microfluidic channel. *BioChip J* **5**: 236–241 http://link.springer.com/10.1007/s13206-011-5307-9.

Persat, A., Nadell, C.D., Kim, M.K., Ingremeau, F., Siryaporn, A., Drescher, K., *et al.* (2015) The mechanical world of bacteria. *Cell* **161**: 988–997 http://dx.doi.org/10.1016/j.cell.2015.05.005.

Putte, P. Van De, Dillewijn, J. Van, and Rörsch, A. (1964) The selection of mutants of escherichia coli with impaired cell division at elevated temperature. *Mutat Res - Fundam Mol Mech Mutagen* **1**: 121–128.

Ramos-León, F., Mariscal, V., Battchikova, N., Aro, E.M., and Flores, E. (2017) Septal protein SepJ from the heterocyst-forming cyanobacterium Anabaena forms multimers and interacts with peptidoglycan. *FEBS Open Bio* **7**: 1515–1526.

Ramos-León, F., Mariscal, V., Frías, J.E., Flores, E., and Herrero, A. (2015) Divisome-dependent subcellular localization of cell-cell joining protein SepJ in the filamentous cyanobacterium Anabaena. *Mol Microbiol* **96**: 566–580.

Rippka, R., Stanier, R.Y., Deruelles, J., Herdman, M., and Waterbury, J.B. (1979) Generic Assignments, Strain Histories and Properties of Pure Cultures of Cyanobacteria. *Microbiology* **111**: 1–61 http://www.microbiologyresearch.org/content/journal/micro/10.1099/00221287-111-1-1.

Rojas, E.R., and Huang, K.C. (2018) Regulation of microbial growth by turgor pressure. *Curr Opin Microbiol* **42**: 62–70 https://doi.org/10.1016/j.mib.2017.10.015.

Rudolf, M., Tetik, N., Ramos-León, F., Flinner, N., Ngo, G., Stevanovic, M., *et al.* (2015) The Peptidoglycan-Binding Protein SjcF1 Influences Septal Junction Function and Channel Formation in the Filamentous Cyanobacterium Anabaena. *MBio* **6**: e00376-15 http://mbio.asm.org/content/6/4/e00376-15.abstract.

Sakr, S., Jeanjean, R., Zhang, C.-C., and Arcondeguy, T. (2006a) Inhibition of cell division suppresses heterocyst development in Anabaena sp. strain PCC 7120. *J Bacteriol* **188**: 1396–1404 http://jb.asm.org/content/188/4/1396.short.

Sakr, S., Thyssen, M., Denis, M., and Zhang, C.C. (2006b) Relationship among several key cell cycle events in the developmental cyanobacterium Anabaena sp. strain PCC 7120. *J Bacteriol* **188**: 5958–5965.

Schlieper, D., Oliva, M. a, Andreu, J.M., and Löwe, J. (2005) Structure of bacterial tubulin BtubA/B: evidence for horizontal gene transfer. *Proc Natl Acad Sci U S A* **102**: 9170–9175.

Schneider, C.A., Rasband, W.S., and Eliceiri, K.W. (2012) NIH Image to ImageJ: 25 years of image analysis. *Nat Methods* **9**: 671 https://doi.org/10.1038/nmeth.2089.

Schumacher, D., and Søgaard-Andersen, L. (2017) Regulation of Cell Polarity in Motility and Cell Division in Myxococcus xanthus. *Annu Rev Microbiol Regul* **71**: 61–78 http://core.ac.uk/download/pdf/10697515.pdf.

Schwedock, J., McCormick, J.R., Angert, E.R., Nodwell, J.R., and Losick, R. (1997) Assembly of the cell division protein FtsZ into ladder-like structures in the aerial hyphae of Streptomyces coelicolor. *Mol Microbiol* **25**: 847–858 https://doi.org/10.1111/j.1365-2958.1997.mmi507.x.

Shieh, Y.-W., Minguez, P., Bork, P., Auburger, J.J., Guilbride, D.L., Kramer, G., and Bukau, B. (2015) Operon structure and cotranslational subunit association direct protein assembly in bacteria. *Science (80-)* **350**: 678 LP – 680 http://science.sciencemag.org/content/350/6261/678.abstract.

Singh, S.P., and Montgomery, B.L. (2011) Determining cell shape: adaptive regulation of cyanobacterial cellular differentiation and morphology. *Trends Microbiol* **19**: 278–285 https://doi.org/10.1016/j.tim.2011.03.001.

Solovyev, V., and Salamov, A. (2011) Automatic Annotation of Microbial Genomes and Metagenomic Sequences. In *Metagenomics and its Applications in Agriculture, Biomedicine and Environmental Studies*. Robert W. Li, pp (ed.). Nova Science Publishers, Inc., pp. 61–78.

Sonnhammer, E.L., Heijne, G. von, and Krogh, A. (1998) A hidden Markov model for predicting transmembrane helices in protein sequences. *Proceedings* **6**: 175–182.

Specht, M., Schätzle, S., Graumann, P.L., and Waidner, B. (2011) Helicobacter pylori Possesses Four Coiled-Coil-Rich Proteins That Form Extended Filamentous Structures and Control Cell Shape and Motility. *J Bacteriol* **193**: 4523–4530.

Springstein, B.L., Arévalo, S., Helbig, A.O., Herrero, A., Stucken, K., Flores, E., and Dagan, T. (2020a) A novel septal protein of multicellular heterocystous cyanobacteria is associated with the divisome. *Mol Microbiol* 1–15.

Springstein, B.L., Woehle, C., Weissenbach, J., Helbig, A.O., Dagan, T., and Stucken, K. (2020b) Identification and characterization of novel filament-forming proteins in cyanobacteria. *Sci Rep* **10**: 1894 https://doi.org/10.1038/s41598-020-58726-9.

Studier, F.W., and Moffatt, B.A. (1986) Use of bacteriophage T7 RNA polymerase to direct selective high-level expression of cloned genes. *J Mol Biol* **189**: 113–130.

Surovtsev, I. V, and Jacobs-Wagner, C. (2018) Subcellular organization: a critical feature of bacterial cell replication. *Cell* **172**: 1271–1293.

Svetlitsky, D., Dagan, T., and Ziv-Ukelson, M. (2020) Discovery of multi-operon colinear syntenic blocks in microbial genomes. *Bioinformatics* **accepted a**.

Typas, A., Banzhaf, M., Gross, C.A., and Vollmer, W. (2012) From the regulation of peptidoglycan synthesis to bacterial growth and morphology. *Nat Rev Microbiol* **10**: 123–136 http://dx.doi.org/10.1038/nrmicro2677.

Ungerer, J., and Pakrasi, H.B. (2016) Cpf1 Is A Versatile Tool for CRISPR Genome Editing Across Diverse Species of Cyanobacteria. *Sci Rep* **6**: 1–9 http://dx.doi.org/10.1038/srep39681.

Urrejola, C., Dassow, P. von, Engh, G. van den, Salas, L., Mullineaux, C.W., Vicuña, R., and Sanchez-Baracaldo, P. (2020) Loss of filamentous multicellularity in Cyanobacteria - the extremophile Gloeocapsopsis sp. UTEX B3054 retained multicellular features at the genomic and behavioral level. *J Bacteriol* JB.00514-19 http://jb.asm.org/content/early/2020/03/31/JB.00514-19.abstract.

Wagstaff, J., and Löwe, J. (2018) Prokaryotic cytoskeletons: protein filaments organizing small cells. *Nat Rev Microbiol* http://www.nature.com/doifinder/10.1038/nrmicro.2017.153.

Weiss, G.L., Kieninger, A.-K., Maldener, I., Forchhammer, K., and Pilhofer, M. (2019) Structure and Function of a Bacterial Gap Junction Analog. *Cell* **178**: 374-384.e15 https://www.sciencedirect.com/science/article/pii/S0092867419306269?via%3Dihub. Accessed August 2, 2019.

Weissenbach, J., Ilhan, J., Bogumil, D., Hülter, N., Stucken, K., and Dagan, T. (2017) Evolution of Chaperonin Gene Duplication in Stigonematalean Cyanobacteria (Subsection V). *Genome Biol Evol* **9**: 241–252 https://dx.doi.org/10.1093/gbe/evw287.

Wickstead, B., and Gull, K. (2011) The evolution of the cytoskeleton. *J Cell Biol* **194**: 513–525.

Wilk, L., Strauss, M., Rudolf, M., Nicolaisen, K., Flores, E., Kühlbrandt, W., and Schleiff, E. (2011) Outer membrane continuity and septosome formation between vegetative cells in the filaments of Anabaena sp. PCC 7120. *Cell Microbiol* **13**: 1744–1754.

Wilson, C.G.M., Magliery, T.J., and Regan, L. (2004) Detecting protein-protein interactions with GFP-fragment reassembly. *Nat Methods* **1**: 255–262.

Wolk, C.P., Cai, Y., Cardemil, L., Flores, E., Hohn, B., Murry, M., *et al.* (1988) Isolation and complementation of mutants of Anabaena sp. strain PCC 7120 unable to grow aerobically on dinitrogen. *J Bacteriol* **170**: 1239–1244.

Yang, R., Bartle, S., Otto, R., Rogers, M., Plamann, L., Hartzell, P.L., and Stassinopoulos, A. (2004) AglZ Is a Filament-Forming Coiled-Coil Protein Required for Adventurous Gliding Motility of Myxococcus xanthus. *J Bacteriol* **186**: 6168–6178.

Yang, Y., Huang, X.-Z., Wang, L., Risoul, V., Zhang, C.-C., and Chen, W.-L. (2013) Phenotypic variation caused by variation in the relative copy number of pDU1-based plasmids expressing the GAF domain of Pkn41 or Pkn42 in Anabaena sp. PCC 7120. *Res Microbiol* **164**: 127–135 http://www.sciencedirect.com/science/article/pii/S0923250812001556.

Young, K.D. (2006) The selective value of bacterial shape. *Microbiol Mol Biol Rev* **70**: 660–703 https://www.ncbi.nlm.nih.gov/pubmed/16959965.

Zhang, C.-C.C., Hugenin, S., Friry, A., Huguenin, S., and Friry, A. (1995) Analysis of genes encoding the cell division protein FtsZ and a glutathione synthetase homologue in the cyanobacterium Anabaena sp. PCC 7120. *Res Microbiol* **146**: 445–455 http://www.sciencedirect.com/science/article/pii/0923250896802907.

Zhang, Y. (2009) I-TASSER: Fully automated protein structure prediction in CASP8. *Proteins Struct Funct Bioinforma* **77**: 100–113.